Tectonophysics
October 2021, Volume 817, Pages 229050 (19p.)
https://doi.org/10.1016/j.tecto.2021.229050
https://archimer.ifremer.fr/doc/00721/83301/

Geodynamic and plate kinematic context of South China Sea subduction during Okinawa trough opening and Taiwan orogeny

Sibuet Jean-Claude [1, 2, 3], Zhao Minghui [1, 4], Wu Jonny [5], Lee Chao-Shing [6, *]

[1] Key Laboratory of Ocean and Marginal Sea Geology, South China Sea Institute of Oceanology, Chinese Academy of Sciences, Guangzhou, China
[2] 44 Rue du Cloître, 29280 Plouzané, France
[3] Ifremer Centre de Brest, B.P. 70, 29280 Plouzané Cedex, France
[4] University of Chinese Academy of Sciences, Beijing 100049, China
[5] University of Houston, Department of Earth and Atmospheric Sciences, Science & Research Building 1, 3507 Cullen Boulevard, Houston, TX 77204, USA
[6] Institute of Applied Geophysics, National Taiwan Ocean University, 2 Pei-Ning Road, Keelung 202, Taiwan

* Corresponding author : Chao-Shing Lee, email address : leecs@ntou.edu.tw

Abstract :

The geodynamics and plate tectonics of the South China Sea (SCS)-Taiwan region since Miocene times are uncertain because the former extent and tectonic configuration of the subducted easternmost SCS along the Manila trench is uncertain. Here we unravel the regional kinematic context from main offshore constraints including published unfolding of the Manila slab from seismic tomography, which provides insight on restoring the subducted part of the SCS. We reconstruct a bayonet-shaped, stepped northern SCS continent-ocean boundary (COB) that consists of a northeastern SCS COB segment we call 'S3', trending N070° that roughly parallels the present SCS shelf; a 350-km long ~N-S trending segment S2 that steps north to Hualien; and, a third segment S1 that extends from east of Hualien beneath the Ryukyu subduction zone trending N085° that ends near Miyako Island in the Ryukyus.

The distance between present COB and S1 gives extension through time in the Okinawa trough, with a maximum of ~100 ± 20 km extension since late Miocene (10 Ma). We interpret S1 as a zone of weakness since ~18 Ma that ruptured from Miyako Island to east of Hualien as a tear fault, with the Huatung basin-Philippine Sea plate (HB-PSP) subducting northwestward between the two sides of the tear fault. The Manila transcurrent fault initiated ~18 Ma ago at the onset of the tear and progressively moved eastward, creating the intra-oceanic Luzon arc, which began collision ~7 Ma ago along the EU margin. From ~7 to 6.5 Ma Taiwan was uplifted west of the Longitudinal valley. The Luzon arc and forearc basins were shortened within the Coastal range. Plate kinematic reconstructions from ~18 Ma to Present are synthesized in terms of continental or oceanic nature of the main PSP-HB and EU entities before their subduction that provide new understanding on Taiwan, PSP-SCS kinematics, and regional histories.

Highlights

► 350-km N-S bayonet-shaped Eurasia (EU) continent-ocean boundary (COB) west of Taiwan. ► EU COBs before and after Okinawa trough opening constrain South China Sea subduction. ► Clockwise Luzon arc rotated blocks collide EU margin before incorporation in Coastal range. ► Kinematic reconstructions synthesize main stages of South China Sea subduction and Taiwan uplif.

Keywords : South China Sea tomography, EU margin bayonet shape, Ryukyu tear fault, Ryukyu slab retreat, less deformed northeastern SCS margin, highly deformed Taiwan margin

1. Introduction and geological setting

1.1. Succinct geological setting

The Taiwan uplift results from the collision of the Eurasian (EU) continental margin with the Luzon arc, which is built on Huatung basin-Phlippine Sea plate (HB-PSP) crust (Fig. 1). Though the arc-continent collision model is well accepted, the mechanism of collision is controversial with a northwesterly or northerly motion of the Luzon arc with respect to EU and a clockwise or counterclockwise rotation of the Luzon arc (first synthesis in Teng (1990)). The onset of Taiwan uplift was inferred to occur sometime between late Miocene and Plio-Pleistocene (Teng, 1990). It was updated by Lin et al. (2002), who established that the foreland basin located west of Taiwan was created by flexure of the elastic continental lithosphere under the Taiwan mountain load and buried loads since ~6.5 Ma, resulting in the tectonic subsidence of the foreland basin (Fig. 2) and the deposition of thick sedimentary sequences. Since the beginning of SCS subduction, the ~NW HB-PSP/EU motion is roughly partitioned east and west of the Longitudinal valley (LV) between 1) ~E-W tensional and compressive features which appear in the Ryukyu subduction zone and 2) parallel compressive ridges trending ~NNE-SSW in Taiwan and ~N-S south of Taiwan (Fig. 2).

East of Taiwan, the Huatung oceanic basin is separated from the oceanic PSP by the Gagua ridge. The HB age is controversial and varies from Early Tertiary (Hilde and Lee, 1984) to Early Cretaceous (Deschamps et al., 2000). As shown by the well-known block diagram of Angelier (1986), the HB and PSP subduct beneath the Okinawa trough (OT), a backarc basin starting to open within the EU continent sometime between ~8 and ~12 Ma ago (Sibuet et al., 2004), and which terminates in the Ilan Plain (northern Taiwan) (Fig. 2). South of Taiwan, the SCS subducts eastward beneath the HB and the western part of the PSP and gives rise to the Luzon arc during middle Miocene or possibly earlier during early Miocene (Chi and Suppe, 1985; Richard et al., 1986; Huang et al., 2018). South of Taiwan, the Luzon arc, which

includes Lutao and Lanyu islands, collides with the EU thinned continental crust (Fig. 2).

From east to west, Taiwan is divided into five major units (Fig. 2): 1) East of the LV, the Coastal range represents the accreted portion of the Luzon arc. It consists of extinct volcanic products, associated remnant forearc rocks and intermingled sediments from intra-arc basins (Huang et al., 2006); 2) The Central range, which includes to the west Miocene slates-turbidites of the eastern part of the Hsuehshan basin and to the east Eocene quartzite-limestone-slate overlying unconformably the Paleozoic-Mesozoic metamorphic basement (Tananao complex) (Huang et al., 2006); 3) The Hsuehshan range, bounded to the east by the Lishan fault, is composed of Miocene meta-sediments belonging to the western part of the former Hsuehshan basin (Sibuet et al., 2004; Huang et al., 2006); 4) The slightly deformed passive EU margin, which includes the western Foothills and Coastal plain; 5) The foreland basin located further west and created by the flexure caused by Taiwan uplift (Lin and Watts, 2002).

1.2. Northerly trending Eurasian margin east and southeast of Taiwan

Following Suppe (1981), the PSP/EU plate convergence in Taiwan is 7 cm/yr in the N305° direction (Seno, 1977), the Coastal range is N016° oriented while the Luzon arc is N-S oriented, implying a 90 km/Ma southward rate of propagation of the collision along the Coastal range (velocity triangle in Fig. 3A). As the migration of Taiwan uplift from north to south of Taiwan became a commonly accepted hypothesis, it was suggested that the Taiwan region displayed all stages of collisional and tensional processes from incipient collision south of Taiwan to active collision in central Taiwan (Suppe, 1981), and to extension after collision in the north of Taiwan (*e.g.* Lallemand and Tsien (1997)).

It is only in 2014 that Mesalles et al. (2014), based on zircon and apatite fission-track ages from sediments in southern Taiwan, showed that the Taiwan uplift had started 7.1 ± 1.3 Ma ago with crustal thickening of the distal thinned continental margin. These observations imply a synchronous initial collision along eastern Taiwan in conflict with the southward-propagation model (Suppe, 1981) (Fig. 3B). One year

later, Lee et al. (2015) confirmed that the Taiwan uplift occurred almost simultaneously along the whole Taiwan orogenic belt. They interpret ~100 zircon fission-track ages collected along the whole Central range between 22.5°N and 24.7°N combined with the 5-6 Ma rapid subsidence observed in foreland basins. They suggest that the Luzon arc located southeast of Taiwan (Hall, 2012) collided the EU margin along a 300-km long ~N-S segment offset as a bayonet the continent-ocean boundaries (COB) of northeastern SCS and eastern EU before the westward propagation of the Ryukyu trench (Fig. 3B).

Although the SCS east of the Manila trench has been subducted and lost, segments of the COB on its missing portion have been inferred from tomographic velocities within the Manila slab (Wu et al., 2016) (Fig. 3C). Segment S1 is defined from south of Miyako Island to Taiwan and segment S3 corresponds to the northeastern SCS COB (Liu et al., 2018). Segment S2 joins S1 to S3, is ~350 km long and roughly parallel to the LV but is not located by the tomographic data because *dVp* velocities within the uppermost 75 to 100 km of the Manila slab are less reliable due to crustal corrections (Wu et al., 2016). While the Luzon arc collides in parallel the EU thinned continental crust in Lee et al. (2015) (Fig. 3B), in our hypothesis, the N-S trending Luzon arc collides the EU continental crust with a 16° angle (Fig. 3C). The velocity triangle shows that along the 130 km of the LV, the rate of propagation of the collision is 240 km/Ma (Fig. 3C), *i.e.* 3 times faster than in Suppe (1981) sketch (Fig. 3A).

Consequently, based on recent geophysical and geological data, the EU COB presented a ~350 km long offset located east of Taiwan before the collision of the Luzon arc. Since Suppe (1981), in most of kinematic reconstructions this lack of offset corresponded to a hidden ~300-km offset as for Angelier et al. (1990) reconstruction where this offset can be suspected but was never mentioned mostly because the Ryukyu trench bends west of Miyako Island.

1.3. Objectives and data used in this study

The aim of this paper is not to understand the complete Wilson cycle of a

marginal basin, but only the present last part of the last Wilson cycle of the SCS. Surprisingly, the disappearance of the SCS marginal basin results in the Taiwan uplift due to the collision of the Luzon arc with the S2 segment of EU margin and the opening of the OT resulting from the HB-PHP northwestward subduction beneath EU. Therefore, the death of the SCS marginal basin is concomitant with the Taiwan uplift and the OT extension occurring simultaneously, at least since ~7 Ma.

One problem faced in this study is the lack of consensus on ages of principal geodynamic events: Amongst them: 1) The age of the end of SCS seafloor spreading between 15 Ma (Briais et al., 1993; Guan et al., 2021) and 20 Ma (Barckhausen et al., 2014). Even if a high-resolution magnetic isochron pattern is available in the SCS East Sub-basin (Guan et al., 2021), large age uncertainties remain for the central East Sub-basin magnetic lineations. 2) The age of initial Luzon arc formation between 13 Ma and 23 Ma (Chi and Suppe, 1985; Richard et al., 1986; Huang et al., 2018) and 3) The age of the onset of OT opening between 8 and 12 Ma (Miki, 1995; Sibuet et al., 1995; Shinjo, 1999; Shinjo et al., 1999; Lallemand et al., 2001). Even if these ages are known with large errors, to avoid repetitions all along the text, the end of SCS seafloor spreading between 15 and 20 Ma will be quoted ~15 Ma (Briais et al., 1993; Guan et al., 2021); the age of initial formation of the Miocene arc between 13 and 23 Ma will be quoted ~18 Ma (Huang et al., 2018); the age of initial OT opening between 8 and 12 Ma will be quoted 10 Ma (Miki, 1995; Shinjo et al., 1999).

Several types of offshore data are used in this study: 1) The swath-bathymetric map between Taiwan and north Luzon (Fig. 4) and a new compilation of swath-bathymetric data in the Bashi Strait (Fig. 5) to better constrain S3 and S2 from 117 to 120.5°E and up to 21°N. 2) the Manila slab tomographic data providing information on the location of the northern SCS COB between 125°E and Taiwan, and on the nature of the subducted crust, before the westward propagation of the Ryukyu subduction zone since 18 Ma (Fig. 6); 3) The processing or re-processing of refraction profiles across the southern portion of S2 showing the present-day presence of the SCS COB (supplementary Fig. S1); 4) The present plate boundary between 125°E and Taiwan will be established by using the available swath bathymetric map of Fig. 7 and

by comparing the multi-channel seismic (MCS) lines (collected on the Ryukyu accretionary prism and forearc basin) re-interpreted by using recently acquired refraction profiles (Fig. 8).

2. Results

2.1. Geometry of the Eurasian COB

The northern SCS COB is poorly defined along segment S2 located within the area where velocity variations are unreliable due to crustal corrections (Liu et al., 2018). On the bathymetric map from southern Taiwan to northern Luzon, partly based on available swath-bathymetric data (Fig. 4), the white hexagons correspond to points where the COB has been clearly identified along segment S3 and along the southern part of segment S2. Starting at 117°E, S3 is defined along MCS profile MGL0905_17 (McIntosh et al., 2014), OBS2016-2 line between OBSs 11 and 12 (Wan et al., 2019), OBS2001 line between OBSs 2 and 3 (Wang et al., 2006), MCS profile MGL0905_20 (Yeh et al., 2012). Along the southern part of S2, 1) the refraction profile T1 (Eakin et al., 2014) has been reprocessed by adding the PmP arrivals and 2) using the PmPs, the interpretation of refraction profile OBS2016-1 has been integrated with the one of refraction profile OBS2016-2 (Liu et al., 2018).

Along T1, the COB has been identified between OBSs 11 and 12 (Fig. 4). West of the white hexagon, *Vp* velocities are those of a thinned continental crust 10-12 km thick as already shown by Eakin et al. (2014). East of the hexagon, the crust dips below the Luzon forearc and arc with a crustal thickness of 6-7 km and *Vp* velocities corresponding to those of oceanic crust (Supplementary Fig. S1). In Eakin et al. (2014) the crust of the Manila slab is not imaged.

Along OBS2016-1, the COB has been identified between OBSs 5 and 6 (Fig. 4). Similarly to refraction profile T1, west of the hexagon, *Vp* velocities are those of a thinned continental crust 7-13 km thick as already shown by Eakin et al. (2014). East of the hexagon, the crust dips below the Luzon forearc and arc with a thickness of the crust reduced to 6-8 km and *Vp* velocities corresponding to those of oceanic crust

(Supplementary Fig. S1).

Thus, south of 21°N, the COB is well identified along the southern part of S2 and the Manila slab is entirely oceanic (Fig. 4). On the other hand, Eakin et al. (2014) model suggests that along T1 (at ~20.5°N), the hyperextended continental crust has recently begun to subduct below the Manila trench while along T2 (~21.5°N) as much as ~100 km of 10-15 km thick, hyperextended continental crust has subducted. However, as the crust of the Manila slab is not imaged along T1 and T2 in Eakin et al. (2014), we question the proposed geometry and the nature of the slab. Unfortunately, the present unavailability of T2 refraction data excludes any reprocessing for the moment.

Fig. 5 is the compilation of swath-bathymetric data collected in the Bashi Strait (between Taiwan and north Luzon) and in the surrounding region from the Gagua ridge to west of the Manila trench. S3, the N070° trending COB segment of the northern SCS margin separates two different portions of the Hengchun ridge. South of S3, the width of the Hengchun ridge is constant from 20.5 to 19.7 °N but decreases by 40% compared with its width at 21°N while its water depth increases (Fig. 5). South of S3, the Hengchun ridge corresponds to the accretionary prism of the intra-oceanic subduction zone, and just north of S3, the Hengchun ridge corresponds to an uplifted portion of the accretionary prism, which starts to be deformed by the Luzon arc collision with EU. Thus, since the onset of S, 30-34 Ma ago, the location of S3 relative to the stable EU has not changed, while S2 is located between the S3-S2 intersection and Hualien located at the northern end of the LV or further east if the distal part of the continental margin has already subducted in the Manila subduction zone. We call $S2_{init}$ and $S2_{final}$ the locations of S2 before the Luzon arc collision and today, respectively.

Based on GPS measurements in north Luzon (Yu et al., 1999), the old reactivated left-lateral Philippine fault zone (PFZ) (Aurelio et al., 1997) (Figs. 1, 4) has an average left-lateral fault slip rate of 35 mm/yr. A similar left-lateral fault slip rate of 30 mm/yr (Yu and Kuo, 2001) was measured between the Coastal range and the Central range. However, Angelier et al. (1997) only observed 1.3 mm/yr of aseismic

slip in the LV. Canitano et al. (2021) suggest that the observed 1.3 mm/yr slip consists of both aseismic and seismic left-lateral shear slip oriented along the LV. The remaining 1.7 mm/yr left-lateral shear motion is absorbed along other thrust faults located inshore or offshore Taiwan, mostly within the accretionary prism (Lee et al., 1997; Conand et al., 2020). Thus, the Manila transcurrent fault (MTF) is a continuous left-lateral shear fault active since 6.5 Ma, which connects the PFZ to the LV (Figs. 1, 4).

Many scientists recognize that a left-lateral shear component was present along most of the major thrusts. For example, based on earthquake focal mechanism, Lewis et al. (2015) suggest that such a left-lateral strike-slip fault exists east of Taiwan, along the Luzon arc. On the swath bathymetric map (Fig. 5) illuminated from the northwest, the present MTF corresponds to an east-facing bathymetric slope, which separates the uplifted accretionary prism (Hengchun peninsula and Hengchun ridge) to the west from the complex forearc features progressively deformed to the north between the Luzon arc and the accretionary prism. An exception exists between 21°30'N and 21°45'N where the collision between the Huatung ridge and the Hengchun ridge is obvious. Here, the MTF follows a canyon roughly N-S oriented (Nayak et al., 2021). Thus, globally, the MTF roughly follows the 121°E meridian and is located on the western boundary of both the flat southern Longitudinal trough (Fig. 5) and further south follows the north Luzon trough (Fig. 4). The MTF is a presently active feature, as shown by a large landslide associated with fresh debris and blocks. Kilometer size blocks are located near 21°15'N, on the western side of the north Luzon trough over a N-S distance of 30 km and a width of 15 km, and also at 19.5°N (Fig. 5). South of 20°N, the north Luzon trough bends to the west of North Luzon and disappears near 17°N (Armada et al., 2020) (Figs 1 and 4). Just north of Luzon Island, in the prolongation of the PFZ and across the north Luzon trough, lies an uplifted N345° trending ridge associated with strike-slip earthquakes attributed to shearing in the offshore prolongation of the PFZ (Armada et al., 2013) (Fig. 4). MCS profiles show that this ridge is active on its eastern side where an associated shear motion is evidenced, and that the north Luzon trough is inactive west and southwest of this

ridge (Armada et al., 2013).

To summarize, the left-lateral PFZ in the Philippines and the left-lateral shear zone in the LV are connected by the MTF (Fig. 4), whose present surface location approximately follows the 121°E meridian. At depth, the MTF corresponds to the plate boundary between the EU and PSP plates. The MTF dips 50° to the east from north of Luzon Island until southern Taiwan and then progressively increases its dip to become almost vertical north of the LV (Ustaszewski et al., 2012). Concerning the northern SCS COB initiated 30-34 Ma ago, S3 is still in the same position today but $S2_{final}$ is also located along the LV where the MTF is almost vertical. $S2_{init}$ was perhaps located a few tens of km further east - much more for McIntosh et al. (2013) - before the collision of the Luzon arc with EU.

2.2. Geometry and nature (oceanic versus continental crust) of the unfolded Manila slab

Wu et al. (2016) have shown that the Manila slab anomaly extended past the Benioff zone to a depth of ~450 km. *dVp* velocities deduced from MITP08 *P*-wave global seismic tomography (Li et al., 2008) are displayed along the unfolded Manila mid-slab (Fig. 6). Velocity contrasts are up to 1% (Liu et al., 2018), *i.e.* not very large. Despite uncertainty, comparison between tomographic models show consistent velocity domains that can be interpreted in several ways (Liu et al., 2018): a) A conservative way in which the subducted part of the SCS with slightly positive *dVp* are oceanic domains (areas B and D in Fig. 6) in agreement with some proposed kinematic sketches (*e.g.* (Huang et al., 2019), and negative *dVp* (areas A, C and E in Fig. 6) are regions with slab windows or hot zones within the Manila slab due to subduction shortly after spreading (Wu and Suppe, 2018). b) A second way in which slightly positive *dVp* are still interpreted as oceanic domains but negative *dVp* correspond to thinned continental domains (Zhao et al., 2019). In the second interpretation, the question is: Is it possible to subduct thinned continental crust without violating isostatic rules? McIntosh et al. (2013) suggest that in the Hengchun peninsula and in the southern Central range, the upper part of the thinned continental

EU crust was underthrusted at the Manila trench and accreted at the base of the accretionary prism, the remaining lower part of thinned continental crust and lithosphere subducting below the forearc to a depth of 120 km. Another possibility is to delaminate the thinned continental crust, the upper part of the crust staying at the earth surface whereas the slab formed by the continental mantle lithosphere including part of the lower crust can subduct as shown in Taiwan (Suppe et al., 2011; Ustaszewski et al., 2012), in northern Banda Sea (Spakman and Hall, 2010) or in the Aegean Sea, north of the Kefalonia Transform fault (Özbakır et al., 2020). Thus, we will interpret the negative *dVp* anomalies as thinned continental crust domains. Our interpretation of Fig. 6 has obvious limitations but is informative given the scale of uncertainty in current SCS geodynamic models. We will show later that such a hypothesis is supported by several recent geological observations.

The spreading flow-lines determined in the East Sub-basin (black lines in Fig. 6) (Sibuet et al., 2016) have been used to rotate the northern COB S (solid red line in Fig. 6). S', the rotated COB (light brown line), fits the southern COB previously identified on the southern margin of the East Sub-basin (green line in Fig. 6). Between the two conjugate boundaries S and S', positive *dVp* values suggest that the whole domain is oceanic including features F and F' considered as artifacts (Zhao et al., 2019). Outside the oceanic domain, negative *dVp* velocity domains A, C and E that we interpret as thinned continental crust are significant features reproduced in four different tomographic models (Liu et al., 2018). Therefore, the subducted SCS seems to have been created by seafloor spreading with the same kinematic parameters as those for the East Sub-basin. If it is true, the eastern boundary of the slab imaged by tomography is not necessarily a plate tectonic boundary. The real eastward extension of the oceanic domain might follow a flow-line similar to that of the East Sub-basin (Fig. 6). The resulting yellow domain would be part of the SCS oceanic domain. As the eastern extremity of S1 is poorly defined in the deepest imaged part of the Manila slab, the SCS eastern boundary can possibly lie a few tens kilometers further east (dashed red lines in Fig. 6). Therefore, despite the uncertainties in interpreting tomographic data, the proposed geometry of the SCS before subduction seems to be

reasonable.

2.3. Location of the continent-ocean boundary before and after southern Okinawa trough opening

The southernmost OT is an atypical backarc basin because the arc volcanism is absent at least from Miocene to Pliocene in the area of Yaeyama Islands (Ishigaki to Yonaguni Islands located in Fig. 7) (Shinjo, 1999). Therefore, Lallemand et al. (2001) suggested that the southern Ryukyu arc was not associated with a subduction zone and that the southern border of the EU passive margin extended to 125°E (south of Miyako Island). Eighteen years after the first tomographic images (Bijwaard et al., 1998) displayed in Lallemand et al. (2001), the unfolded Manila slab (Wu et al., 2016) with mid-slab *dVp* values gives a much better image of the extent and nature of the whole SCS. For comparison, the contour of the oceanic domain manually determined by Lallemand et al. (2001) from Bijwaard et al. (1998) tomographic images (thin dashed lines in Fig. 6) roughly follows the boundaries of our SCS domain with a maximum gap of 150 km. The northwestern portion of the Lallemand et al. (2001) oceanic domain (continuous black line) was interpreted as the present-day trace of a tear fault (T1), which had propagated in direction of Taiwan, and then inside of the EU continental domain (Lallemand et al., 1997; Lallemand et al., 2001). The Lallemand et al. contour is oblique to S1 and merges S1 east of Taiwan.

Near 23.6°N; 125.5°E (point **d** in Fig. 7) the Ryukyu trench changes orientation and the width of the Yaeyama ridge (YR in Fig. 7) progressively increases in the direction of Taiwan. Gravity high appears in the forearc off Miyako Island, where the Luzon-Okinawa fracture zone (LOFZ) system bends and becomes parallel to the Ryukyu trench. Segment **ad** (thick black line in Fig. 7) oriented N343° corresponds to the northern portion of the eastern boundary of the SCS oceanic domain delineated in Fig. 6. It is in this area that the SCS subduction would initiate and then propagate westward.

To establish where is located today the southern boundary of the thinned continental crust, we have compared a series of five deep MCS profiles (named A to E

in Fig. 7) extending across the Ryukyu forearc and the HB-PSP oceanic crust. They are high quality MCS profiles (Fig. 8) recorded by the *Maurice Ewing* and *Marcus G. Langseth* seismic research vessels during the TAICRUST and TAIGER cooperative programs (Liu et al., 1997; Lester et al., 2013). 6-km long streamers and large low-frequency seismic sources (>6000 in^3) were used in order to get deep penetration. Wide-angle reflection and refraction seismic data were acquired with 7 and 19 OBSs on profiles D and E, respectively. The basement (thinned dashed lines in Fig. 8) is reliable on profile E where the OBS spacing is 7.5 km (Klingelhoefer et al., 2012). On profile D, the oceanic basement beneath the Yaeyama ridge is not so well defined because the OBS spacing is 25 km along this profile (Wang et al., 2001).

The Ryukyu trench changes orientation at ~125.5°E longitude from N082° in the west to N052° in the east. In the east, the trench is quasi-linear and the present direction of convergence is almost perpendicular to the trench azimuth up to the Daito ridge (Fig. 7). Above the plate interface (Fig. 8A), the Ryukyu forearc basin thickness exceeds 6 s two-way travel time (twtt), making it difficult to identify the oceanic or continental nature of the underlying basement marked ???? in Fig. 8A. An outer ridge marks the seafloor outcrop of the splay fault system and separates the landward uplifting inner wedge from the oceanward outer wedge characterized by folded structures (Hsu et al., 2013). The origin of this 500-km long south Ryukyu mega-splay fault system may be ascribed to the resistant subduction of the trench-parallel LOFZ (Fig. 7) (Hsu et al., 2013).

In contrast, no similar splay fault system is found west of 125.5°E. The four seismic profiles (Figs 8B to 8E) display very similar images. From Profile B to Profile D, the Yaeyama sedimentary ridge increases in width from 0 to 60 km and in thickness above the oceanic crust from 5.5 to ~7 s twtt, concomitantly with the increase of thickness of the undeformed sediments on top the oceanic crust from 1 to 3 s twtt before their incorporation into the Yaeyama ridge. Slip partitioning, caused by oblique convergence, is localized along a major dextral transcurrent fault located at the rear of the Yaeyama ridge (Fig. 2) (Lallemand et al., 1999). On MCS profiles B to D, the basement of the Ryukyu forearc below the Nanao basin is irregular but always

clearly defined, including where it abruptly terminates against the buried part of the Yaeyama ridge (continuous black lines on Figs. 8B to 8E). *P*-wave velocities obtained along Profiles D and E show that the nature of the forearc crust is continental (Klingelhoefer et al., 2012), which is confirmed by another refraction profile (Arai et al., 2017) located close to profile B.

The southern extremity of the Ryukyu forearc continental crust is the present location of the COB and is shown by a vertical arrow on Figs. 8B to 8E. The COB is not exactly coincident with the location of the transcurrent fault on the sea-bottom, at the contact of the Yaeyama ridge with the undeformed Nanao basin. At depth, the COB is located between 0 and 8 km south of the transcurrent fault. Along profiles B to E, the locations of the COB appear as small circles located up to a few kilometers south of the rear of the Yaeyama ridge (Fig. 7). However, west of Profile E, the southward limit of the Ryukyu forearc basement is difficult to identify, suggesting the western end of $S1_{init}$ might be located in **b** (Fig. 7), ~40 km east of Hualien.

3. Discussion

3.1.Okinawa trough opening

3.1.1. Role of tear fault in Okinawa trough opening

The COB is a zone of weakness between an oceanic domain and the edge of the adjacent continent. It might become a zone of rupture when a compressive stress is applied (Sibuet et al., 1996). Depending on the convergence angle, a subduction zone or a sheared margin can be formed. S1 is such a zone of weakness. It ruptured along segment **ab** (Fig. 7) as a tear fault (T1), the HB-PSP subducting toward the northwest between the two lips of the tear fault and propagating westward from point **a** to point **b**. At the rear of the Yaeyama ridge (purple dashed line in Fig. 7), the present COB (**db**) changes trend in **f** from N274° (segment **df**) to N309° (segment **fb**). This change of trend in **f** might be linked either to an increase of the amplitude of the HB-PSP/EU vector or to the beginning of the Luzon arc collision with the EU margin.

$S1_{init}$, emplaced 30-34 Ma ago, well before the OT opening, is located north the

present location of the COB (Fig. 7). The initial and present COBs intersect in **b**, located 40 km east of Hualien and display a ~22° angle between them. The N-S distance between the two COBs is 100 km south of **a** (close to Miyako Island), also 100 km south of **h** (just east of Ishigaki Island), 60 km north of the Gagua ridge and 30 km in **f**. If the present COB is defined with less than a 10-km accuracy, on the other end the accuracy in the location of COB $S1_{init}$ might be several tens of kilometers. Consequently, the extension of 100 km between points **a** and **d** is known with a ~40 km accuracy.

Another way to define the OT extension is to compute the extension along profile P1 (Fig. 7) by using refraction data (Sibuet et al., 1995) and a crustal model in local isostatic equilibrium. The Moho is at a depth of 18 km at the intersection of profile P1 with the OT axis for Hirata et al. (1991), at 15 km at the intersection between a refraction profile shot along the OT axis (Lee et al., 1980) and Profile P1, and 12 km beneath the rift axis along a refraction profile with OBSs every 6 km almost coincident with profile P1 (Arai et al., 2017). The total extension calculated along Profile P1 is 82 km in the first case, 99 km in the second case (Sibuet et al., 1995) and ~115 km in the third case *i.e.* 100 +/-20 km, a value comparable to the distance between points **a** and **d** or **h** and **h'** (100 +/-40 km).

3.1.2. Timing of Okinawa trough opening

The timing of the OT opening was mainly established during the late 90's (Miki, 1995; Sibuet et al., 1995; Shinjo, 1999; Shinjo et al., 1999). Many volcanic and sedimentary rocks collected on the islands of the Ryukyu arc (located in Figs. 1 and 7) from southern OT (Ishigaki, Miyako islands), middle OT (Okinawa, Kume islands) and northern OT (Amami, Tokuno islands) were analysed for ages and paleomagnetic properties (Miki, 1995; Shinjo, 1999; Shinjo et al., 1999). The southern part of the Ryukyu arc, including the Yaeyama Islands (Ishigaki to Yonaguni islands), rotated ~25° clockwise from 10 to 6 Ma (Miki, 1995). However, during the same period of time, Miyako Island had undergone almost no rotation, and the islands of the Ryukyu arc located in the middle and northern OT did not rotate since 17 Ma. All the islands

located north of Miyako Island drifted away from EU (with a pole of rotation located far away) showing the whole OT opened during the same 10 to 6 Ma period of time (Miki, 1995; Sibuet et al., 1995; Shinjo, 1999; Shinjo et al., 1999). After a period of cessation of tectonic activity emphasized between 6 and 1 Ma (Miki, 1995) or between 6 and 2 Ma (Sibuet et al., 1995; Shinjo et al., 1999), a second phase of limited extension occurred in the OT with the formation of overlapping en-échelon grabens sometimes intruded by basaltic ridges (Sibuet et al., 1987; Misawa et al., 2020). Thus, the whole extension near point **a** (~100 km +/-20 km) includes something like ~10 km of extension since the uppermost Pliocene (1 or 2 Ma).

If the collision of the Luzon arc with the EU margin started ~7 Ma ago and if Taiwan was already uplifted 6.5 Ma ago, it means that the OT opening is not related to the Taiwan orogeny. After the cessation of OT opening 6 Ma ago, the OT opening resumes 2 or 1 Ma ago with the propagation of the OT tip inside Taiwan (Ilan Plain) (Sibuet et al., 1995; Shinjo et al., 1999; Hsiang et al., 2018). Though S2 does not exist north of Hualien because it is connected to S1, the present MTF continues to the north along the EU/HPSP plate interface. Ustaszewski et al. (2012) shows that the EU/HB-PSP plate interface is dipping to the west in the southern part of the longitudinal valley, is almost vertical near Hualien and then overturns further north changing direction to pass below the OT tip and below the Tatun volcano (Figs. 2 and 9D). The HB-PSP slab passes below northern Taiwan ~30 km north of Hualien where the slab is at a depth of ~50 km. Below the Tatun volcano, the top of the HB-PSP slab is definitely below the EU lithosphere, at a depth of 150 km (Ustaszewski et al., 2012).

The N300° oriented seismic refraction profile T6 (Van Avendonk et al., 2016) (located in Fig. 9A) cut across Taiwan just south of the Ilan plain. Based on the seismicity recorded in the 35-km thick crust and deeper, a near vertical strike-slip shear zone was identified along the coast of northeastern Taiwan. This shear zone corresponds to the northward prolongation of the MTF. Further northwest Van Avendonk et al. (2016) confirms that the HB-PSP edge is located below the Tatun volcano and that the HB-PSP oceanic lithosphere and associated deep seismicity

appear underneath the EU continental crust and lithosphere. Both Van Avendonk et al. (2016) and Ustaszewski et al. (2012) confirm that, since 1 or 2 Ma, the OT opening resumes with the formation of the Ilan Plain due to the progressive impingement of the HB-PSP oceanic lithosphere beneath the 40 km thick EU crust (Fig. 2).

3.1.3. Opening mechanism of the Okinawa trough

If there is a general consensus recognizing that the SCS subduction started simultaneously with the end of SCS opening, we cannot exclude that the SCS subduction and Luzon arc formation started 18 Ma ago while the SCS opening was still underway until 15 Ma, preventing to properly image the full SCS oceanic extent. Several examples of subducting active or recently active spreading ridges exist in the east Pacific basin (Sisson et al., 2003) and include the oblique subduction of the South Chile spreading ridge below the Andes and Patagonia since 17 Ma (Boutonnet et al., 2010). Figs 9A and 10A show the SCS in contact with the HB-PSP before the onset of OT opening. In our retained scenario, subduction initiated 18 Ma ago along the eastern flow-line of SCS (N343° trending segment **ad** and its southern prolongation in Figs 6 and 7). The initial plate boundary between the SCS and the HB-PSP is the Manila transcurrent fault (MTF). The HB-PSP northwestward motion with respect to EU resulted in the formation of the Manila accretionary prism and Manila trench (Fig. 10B). East of the MTF, the HB-PSP (dark blue in Fig. 9A) is everywhere older than the adjacent SCS oceanic domain.

Since the onset of SCS opening (30-34 Ma), a shear zone, starting in **a** (Figs. 6 and 7), was active during SCS spreading and was progressing in the S-SE ward direction. It is along this shear zone (dashed red line starting in **a** (Fig. 6)) that the subduction plate boundary initiation has focused. The younger oceanic plate, which includes the SCS, subducted westward below the HB-PSP oceanic plate. Only a few examples of spontaneous subduction initiation with the downgoing plate being the youngest are observed in the Hjort, Tiburon and Barracuda subduction zones (Arcay et al., 2020). For isostatic reasons, the oldest oceanic plate underthrusts the younger. Here, prior subduction initiation, the HB-PSP oceanic plate was already subducting

below EU, explaining why the younger plate was unable to subduct below the HB-PSP oceanic plate in the north. Since the beginning of SCS subduction (~18 Ma ago) and the beginning of Luzon arc collision with the EU margin (~7 Ma ago), the MTF moved ~400 km to the west (Fig. 9A). To tear S1 between ~18 and 10 Ma, the PSP had to move in a slightly more westerly direction than the N343° direction of the eastern boundary of the SCS (Fig. 9A). During the ~18-10 Ma period, the Luzon arc formed continuously as an intra-oceanic arc created inside the oceanic HB by subduction of the SCS oceanic crust below the HB-PSP oceanic crust.

As distances between points **a** and **d** and points **h** and **h'** are the same (~100 km), no extension occurred in the OT during the tear of S1 from point **a** located south of Myiako Island to point **h** located just east of Ishigaki Island (Fig. 7) *i.e.* from 18 to 10 Ma (Figs. 9B and 10B). Since 10 Ma, the HB-PSP/EU motion changed direction for a more westerly direction than previously, drastically increasing the eastward SCS subduction rate below the HB-PSP (Figs. 9B and 10B). Assuming **bh** and **bh'** are straight segments, **hh'** represents the amount of OT opening since 10 Ma and the **bhh'** triangle represents the variation of OT opening in the southwestern OT since 10 Ma. Segments **ee'** and **e1e1'** (~100-km long), located in the northern prolongation of segments **ab** and **hh'**, have been superposed to the OT bathymetry (Fig. 7). The **e1ge1'** triangle approximately represents the *in situ* amount of OT opening (or extension) since 10 Ma in the southwestern OT, and the area between broken lines **ge1ee2** and **ge1'e'e2'** (Fig. 7) the extension in the whole OT. In fact, the extension occurs in a wider domain, which includes the northern and southern OT continental slopes in the southern OT and a much wider domain in the middle and northern OT. This scheme simply explains the triangular shape of the southwestern OT. It does not require that Miyako Island had to rotate 25° clockwise, which would have implied the presence of a shear tectonic boundary along the NW-SE oriented Miyako depression located at mid-distance between Miyako and Okinawa Islands as suggested by Miki (1995). To avoid a too large opening in northern OT, this shear tectonic boundary was supposed to decouple the OT opening in the southwestern OT from the one in the central and northwestern OT (Miki, 1995).

If we assume that the southern portion of Ryukyu arc, including Yaeyama islands from Yonaguni to Ishigaki islands (Figs. 10A and 10B), rotated around a pole located at the tip of the Ilan plain, to get a rotation of 100 km for Ishigaki Island, the southern Ryukyu arc must rotate 20° compared with the ~25° clockwise rotation (Miki, 1995). Miyako Island and the Ryukyu arc further north moved 100 km to the N-NW around a pole of rotation located at 90° in the W-SW direction (Figs. 10A and 10B). ~7 Ma ago (Fig. 10C), we roughly estimate that 75% of the OT opening was completed: The southern Ryukyu arc rotated 15° around the same pole and from Ishigaki Island to the northeast, the OT opening was 75 km. Since ~7 Ma ago, the remaining 25% of OT opening resulted in an additional rotation of 5° for the southern Ryukyu arc and 25 km of extension from Ishigaki Island to the northern OT (Fig. 10D).

Between ~18 Ma and 10 Ma ago, the OT was not opening, suggesting that the Ryukyu slab was a non-retreating slab during this period. It evolved to a retreating slab from 10 Ma to 6 Ma, which might be possibly caused by a SE-NW absolute motion of EU with respect to the Ryukyu trench (Wu et al., 2016). A second period during which the OT ceased to open was identified from 6 to 1 or 2 Ma, suggesting the Ryukyu slab was again a non-retreating slab during this period. After this period of quiescence, the OT opening resumes 1 or 2 Ma ago, the Ryukyu slab being again a retreating slab until today.

More than 90% of post-spreading volcanism in the SCS oceanic domain was emplaced along the East sub-Basin extinct spreading ridge during a ~N-S tensional episode occurring 6-10 Ma ago (Pautot et al., 1986; Pautot et al., 1990; Zhao et al., 2018). This post-spreading volcanism could possibly extend along the extinct spreading center in the already subducted part of SCS until ~125°E (Figs. 9B and 10B). As the OT opening occurred during the same period of time, the intraplate SCS post-spreading volcanism might be related to the SE-NW absolute motion of EU and not necessarily driven by the Hainan plume activity, even if the East sub-Basin alkali basalts of OIB-type are explained by a buoyancy driven partial melting mechanism (Zhao et al., 2018).

Though numerous uncertainties exist concerning the age of the different events,

the direction and amount of OT opening and the location of $S1_{init}$, we have now a reasonable model for the OT opening. In the following section we will examine the geodynamic context of the Luzon arc collision with the EU margin.

3.2. Taiwan uplift

3.2.1. Geometry and nature of the ~N-S segment of the Eurasian margin

In Taiwan, two hypotheses are considered concerning the width of the transitional crust before collision: 1) The Hsuehshan trough located approximately below the Hsuehshan range rifted during Eocene to early Oligocene (Teng et al., 1991). It dips eastward in direction of the pre-Mesozoic metamorphic Tananao complex containing high pressure thrust sheets that were emplaced during the Luzon arc collision with the EU margin (Teng et al., 1991). Thus, before ~7 Ma the ~50-km wide margin of the ~N-S segment was lying approximately at the emplacement of both the Hsuehshan and Central ranges and was bounded to the south by the prolongation of the Yichu fault, which possibly extended eastward below the Western foothills until the Hsuehshan range (Brown et al., 2017). 2) The Lishan fault, located between the Hsuehshan and Central ranges, is considered as a reactivated extensional fault (Fisher et al., 2002; Simoes et al., 2007). It is a zone of weakness located at the hinge line of the northern segment of EU margin, which would have been affected by plate bending at the beginning of collision (Lester et al., 2012). In Fig. 9, the second hypothesis is favored. Since it is not known how the Lishan fault joins the questionable eastern extremity of the Yichu fault, we have followed a N309° direction to connect the southern end of the Lishan fault to the eastern extremity of the Yichu fault supposed to be at the intersection between the western Foothills and the Coastal plain (Fig. 9A).

3.2.2. Geometry and nature of the northeastern South China Sea margin

The northeastern termination of the SCS margin ends in southwest Taiwan (Fig. 9). Today, this domain is limited by the present location of $S2_{Final}$, *i.e.* the boundary with the Luzon arc and forearc features to the east, S3 to the south and the Yichu Fault

to the northwest. The Yichu Fault is the boundary between the transitional domain and the ~30-km thick EU continental crust (Nissen et al., 1995) where several elongated tensional basins were formed during Paleocene and Eocene (*e.g.* (Sibuet et al., 2004)), and are now filled with sediments.

Many tilted basement blocks capped by their overlying pre-rift sedimentary cover and soling out on mid-crustal detachment faults (Lester et al., 2012; Yeh et al., 2012; McIntosh et al., 2014) are generally NE trending, display fan-shape synrift strata and define a ~300 km wide rifted continental margin (Fig. 9A). The mid-crustal detachment located at the base of the 4 to 10-km thick upper brittle crust was probably overlying a ductile lower crust during rifting. The major ~NE trending features of the transitional crust are the failed rift with its crust reduced to less than 5 km and an 18-km thickened crust located north of the S3 (McIntosh et al., 2014). Between the detachment fault and the Moho, the lower crust is 2 to 5-km thick and generally includes a 1 to 2-km thick lower basal unit (Eakin et al., 2014; Lester et al., 2014). Several post-rifting seamounts or volcanic ridges of different ages, which uplift the lower series of post-rift sediments and numerous sills located at different post-rift stratigraphic levels are observed in the transitional crust (Yeh et al., 2012; McIntosh et al., 2014) and interpreted as volcanic intrusions through the thinned continental crust (Yeh et al., 2012).

These observations suggest that the northeastern SCS margin present characteristics similar to those of wide basins or wide continental margins (excluding those with serpentinized mantle exhumation) as the Basin and Range province (*e.g.* (Wernicke, 1985)), the Aegean rift (*e.g.* (Jolivet and Brun, 2010)) or the Woodlark basin (*e.g.* (Taylor et al., 1999)) where detailed cross-sections show the relations between detachment faults soling at mid-crustal levels, ductile lower crustal deformation, metamorphic core complexes, late synrift and postrift extensional intrusions. The temperature of the northeastern SCS lithosphere was high enough (~75 mW/m^2 (He et al., 2001)) to develop large-scale flows of lower crustal material and the boudinage due to associated thermal instabilities.

3.2.3. West Taiwan foreland basins

The West Taiwan foreland basin formed since 6.5 Ma by flexure in front of the Taiwan orogeny (Lin and Watts, 2002; Lin et al., 2003). Fig. 9C shows the depth to the base of the foreland sequence (Pan et al., 2015) already underlined in Fig. 2. In the north, the 2-km isobath closely follows the shape of the Western foothills (Lin and Watts, 2002) showing that the foreland basin has a clear relationship with the Taiwan mountain load. In fact, west of central Taiwan, flexure modeling shows that the subsidence of the foreland basin is due to a combination of subsurface and buried loads due to overthrusting of the lower crust on the upper crust (Lin and Watts, 2002). The reactivated Lishan fault has predated the arc-continent collision and might have focused the bending of the transitional crust at the onset of Luzon arc collision at ~7 Ma. If this is true, after incorporation of this initial flexural basin in the Taiwan orogen between ~7 and 6.5 Ma, a secondary foreland basin might have developed 6.5 Ma ago further northwest as the consequence of surface loading and buried loads.

At the intersection with the Yichu fault the foreland basin isobaths change trend and follow the direction of the Yichu fault. Along the Yichu fault, the foreland basin is deeper than west of Central Taiwan and the depth to the base of the foreland sequence dips too steeply to be explained by elastic plate models. After the main Paleogene rifting episode, the margin and in particular the Tainan basin experienced two more recent rifting events during the ~30-21 and ~12.5-6.5 Ma periods, weakening the underlying lithosphere (Lin et al., 2003). For Lin and Watts (2002) the development of the southern foreland basin is strongly influenced by the thermo-mechanical structure of the underlying passive margin. However, we rather follow Lester et al. (2012) who suggest a formation of the southern foreland basin by bending of the transitional crust at the onset of the Luzon arc collision with EU. This hypothesis better explains the normal faulting of the basal foreland surface, the normal faults which highly dissected the overlying sediments and the location of the deepest part of the southern foreland basin close to the intersection with the northern segment of EU margin.

3.2.4. How did the Luzon arc collide with the EU margin since ~7 Ma?

The Luzon arc started to form ~18 Ma ago as recorded in the Lanyu volcanic island where calcareous sediments interbedded in the arc volcanic rocks were dated 18 Ma, coeval with the early activity of the arc and confirming earlier K-Ar dates (Chi and Suppe, 1985). Between ~18 and ~7 Ma, the arc and forearc basin formed continuously. The first and rapid collision of the Luzon arc with the N016° oriented EU margin resulted in the ~7 to 6.5 Ma obduction of the Luzon arc (Coastal range) and the uplift of the Central range, Hsuehshan range and Western foothills. Starting 6.5 Ma ago, the sub-aerial erosion of Taiwan provided sediments transported westward in the foreland basin, in the south Luzon trough forearc basin (Huang et al., 2018) and then in the northern Luzon trough. The corresponding sedimentary sequences S1 (6.5-5.8 Ma), S2 (5.8-3 Ma) and S3 (3-1 Ma) deposited in the south Luzon trough forearc basin are now intermingled with the eruptive volcanic agglomerates of the Tuluanshan formation in the Coastal range (Huang et al., 2018).

East of the MTF, between S3 and Taitung (Fig. 5), lie: 1) the Huatung ridge, a tectonized unit which increases in width northward, 2) the north Luzon trough, a forearc basin squeezed north of 21°15'N up to north of Lutao Island and uplifted between the Huatung ridge and the Luzon arc, 3) the southern Longitudinal trough now filled with sediments and 4) the Luzon arc. All forearc features located between the MTF and the Luzon arc are considered as forearc basins and forearc blocks (McIntosh et al., 2013; Eakin et al., 2014; Huang et al., 2018). East of the Huatung ridge, the eastward verging backthrust (the white line with triangles in Fig. 5) was active during the past 1 Ma (Huang et al., 2018). Thus, between the double vergence system, the Huatung ridge uplift is probably one element of the upper plate shortening. Other elements of shortening include the simultaneous uplift of the termination of the north Luzon trough squeezed between the Luzon arc acting as a buttress and the colliding Huatung ridge and Hengchun ridge from 21.3°N and 22°N, and the significant uplift of the Hengchun ridge and Hengchun peninsula.

Since 6.5 Ma, the portion of Coastal range already formed at the onset of the collision was moving along its own trend with respect to EU, *i.e.* ~200 km or ~85 km

northward if the left-lateral shear velocity along the LV is ~3 cm/yr or ~1.3 cm/yr, respectively. In other words, today, the first created 130-km long segment of Coastal Range is already subducted or only partly subducted. Thus, the Coastal range was neither the initial portion of Coastal range emplaced 6.5 Ma ago nor obducted along its whole length 1 Ma ago as suggested by Huang et al. (2018). Paleomagnetic data show that Lutao and Lanyu Islands rotated ~30° clockwise during the past 1 Ma (Zhao et al., 2016), suggesting that even the Luzon arc buttress is deformed in its northern part (Fig. 5B). Since ~6.5 Ma, new portions of Luzon arc were probably rotated and accreted south of the Coastal range, pushing to the north the oldest portions of Coastal range where they are subducting with the HB-PSP as part of the Ryukyu slab. The proposed process would take place step-by-step, reflecting the extreme complexity of the geodynamic evolution not only of the Coastal range but also of the adjacent Central range.

Thus, since ~7 Ma, due to the NW HB-PSP plate convergence with respect to EU, the motion is partitioned between the ~N-S left-lateral shear motion along the MTF and the E-W compression. The compression results in shortening and uplift of the accretionary prism west of the MTF and of the forearc features and the northern part of the Luzon arc to the east (Figs. 5 and 9C). West of the MTF, the northern segment of margin located north of Taitung is narrow, quickly and highly deformed by the Taiwan uplift, the Tatajo complex playing the role of buttress with respect to the emplacement of the Coastal range east of the MTF. The 16° angle between the N345° trending Luzon arc and the ~N-S trending MTF, is at the origin of a constant squeeze of forearc features due to the northwestward motion of the Luzon arc with respect to the fixed EU since ~7 Ma. Thus, a ~100 km E-W component of shortening might have occurred in the upper plate south of Taitung since ~7 Ma, at the expense of the EU/HB-PSP subduction. A similar shortening occurs north of Taitung as suggested by the ~60 km secondary subduction occurring east of the Coastal range during the last 1 Ma (Yu-Huan Hsieh, personal communication, 2020), reducing the subduction component of the same amount.

3.3. Plate kinematic reconstructions at ~18 Ma, 10 Ma, ~7 Ma and Present: Geodynamic implications

3.3.1. Plate kinematic methodology

Kinematic reconstructions of Wu et al. (2016) and Hall (2012) are in two different mantle frames, which result in additional northwestward PSP motions relative to EU (*e.g.* ~200 km since 18 Ma in Wu et al. (2016)). Paleomagnetic data are in a paleomagnetic reference frame, which differs from the above mantle reference frame. In addition, north Luzon and PSP may have moved together until very recently (*e.g.* 5 Ma for Hall (2012)). Therefore, PSP paleomagnetism may not be reflective of north Luzon motion for the last 18 Ma. In contrast, kinematic reconstructions of Figs. 9 and 10 are relative to a fixed EU, since EU is slow moving and its motions since the Miocene are not well-quantified. Therefore, to improve our kinematic reconstructions, we will use two constraints: the north Luzon paleomagnetic inclinations (Queaño et al., 2007) to quantify the north Luzon variations in paleo-latitudes, and the location of the MTF since 18 Ma (Fig. 9) to define the E-W motions of north Luzon. In this scheme, north Luzon is shown without any clockwise rotations with respect to PSP since 20 Ma.

The observed inclinations of primary magnetization in north Luzon suggest that starting from the late Oligocene-early Miocene, north Luzon moved northward by 10-15° (Queaño et al., 2007) with respect to EU supposed to be fixed. Fitting a straight line across the paleo-latitude data points (Supplementary Fig. S2) gives ~10° of linear latitudinal variation since 18 Ma. In the E-W direction, the previously established velocity motion of the MTF since 18 Ma (Fig. 9), gives the second constraint to define the north Luzon motion with respect to EU.

The complex geodynamic pattern described above is tentatively synthetized in four kinematic reconstructions (Fig. 10). These kinematic reconstructions are different from what was previously published (except Mesalles et al. (2014) and Lee et al. (2015)) mostly because the ~350-km bayonet offset of the EU margin established from tomographic data brings new constraints not only on the development of the tear fault T1 and associated OT opening but also on the collisional processes of the Luzon

arc with the EU margin. The four kinematic reconstructions synthesize the main steps of the evolution of the HB-PSP/EU motion since the onset of SCS subduction. The SCS oceanic domain is initially bounded by COBs S (red dashed lines) and S' (light brown dashed lines), the COB of the SW basin (green line) and the MTF to the east. As seen before, the location of $S2_{init}$ before and during SCS subduction is poorly constrained but is located within the grey area of Fig. 6, that is probably no more than ~40 km east of Hualien. Outside the SCS oceanic domain B, except the two domains in green (C and E in Fig. 6), the rest of the subducted domain is oceanic as domain D (Proto-SCS?) defined in Fig. 6, the northern portion of the oceanic East Asian slab (Wu et al., 2016) and the suggested eastern extension of Sulu Sea (Fig. 10A). Another limitation in the kinematic reconstructions is the MTF trending N343° in Fig. 10A, assumed to remain unchanged in Figs. 10B and 10C, while almost N-S trending in Fig. 10 D.

East of the Luzon arc lies the HB represented as a 100-km wide linear basin parallel to the Manila transcurrent fault bounded by the Gagua ridge to the east, and extending from north Luzon to the Ryukyu trench (Fig. 10A) to the north. As established above, the HB-PSP subducted beneath EU at 55 mm/yr in the NNW direction from ~18 to 10 Ma and at 82 mm/yr in the NW direction since 10 Ma as summarized in Fig. 10D with the north Luzon locations corresponding to each reconstruction.

3.3.2. Geodynamic implications of plate kinematic reconstructions

By closing the SCS oceanic area 30-34 Ma ago, Domain C was located at the corner between segments S1 and S2, suggesting that this portion of thinned continental domain was attached to the EU margin. At the end of SCS spreading, Domain C was located at the corner between S'1 and S'2 (Fig. 6). In Figs. 10A and 10B, Domain C is adjacent to a portion of East Asian slab (Wu et al., 2016) to the east and to the proto-SCS defined in Fig. 6 to the south. We suggest that, between ~10 and ~7 Ma, Domain C disappeared by subduction below the Manila trench, with the upper part of the thinned continental crust accreted against or below the sedimentary prism

and the remaining part of the thinned continental crust and lithosphere incorporated in the Manila subduction zone. Since the end of SCS spreading and during ~10 Ma, Domain C was located ~500 km S-SE of present Taiwan. This is consistent with detrital zircons and paleocurrents within the Loshui formation sediments (10-12 Ma) at the Hengchun peninsula, that indicate northward flow of sediments from a rifted continental fragment of Cathaysia affinity located to the south (Tsai et al., 2020). Overriding of the thinned continental crust of Domain C (Fig. 10C) by the Luzon arc-HB-PSP may have produced additional late Miocene-aged collisions to the south, between Taiwan and north Luzon and possibly the eastward indentation of the Manila subduction zone presently observed at 20°N (Fig. 10D).

Lavas recently collected on the Gagua ridge at 22°N are typical of subduction-related arc magmatism (Qian et al., 2021). The ages of trapped zircon also match the ages of zircons recovered from the Cathaysian block, southern China. The Mesozoic age peak (250 Ma) of the Gagua ridge zircons can possibly be related to widespread contemporaneous magmatic rocks in southern China, while zircon age peaks (~0.75 Ga and ~2.45 Ga) are largely consistent with those for zircons from Cathaysia block. Therefore, the Gagua ridge zircons most likely originated from the Cathaysian block. Another sliver of Cathaysian continent affinity was found within the Coastal range (Luzon arc basement) in Taiwan (Shao et al., 2015). Similar ages at 220 Ma, ~0.73 Ga and ~2.50 Ga also suggest Cathaysia-type sources. In both interpretations, the role of continental material that rifted away from the Eurasian margin is highly suggested (Shao et al., 2015; Qian et al., 2021). In our model, Domain C of Cathaysian affinity drifted about 700 km to the southeast during the SCS opening and then subducted eastward in the Manila subduction zone between ~10 and ~7 Ma (Fig. 10). The depleted mantle wedge-derived magmas picked up the continental zircons during their ascent along the corresponding parts first of the Luzon arc between ~10 and ~7 Ma and then further east along the Gagua ridge possibly between ~2 and ~5 Ma, as deduced from geometric considerations (Fig. 10). Belonging now to the HB-PHP moving NW-ward, the Luzon arc accreted to EU in the Coastal range (Chimei igneous complex (Shao et al., 2015)) and the Gagua ridge

(sampled at 22°N (Qian et al., 2021)) moved to its present location.

The second domain of thinned continental crust is Domain E located south of S'3, between the proto-SCS and north Palawan. Domain E could be considered as the E-NE continuation of the continental crust of North Palawan. Domain E would have subducted below the Manila accretionary prism since 3-4 Ma (Figs. 10C and 10D). As for Domain C, Domain E would have disappeared by subduction below the Manila trench, with the upper part of the thinned continental crust accreted against or below the sedimentary prism and the remaining part of the thinned continental crust and lithosphere incorporated within the Manila subduction zone.

The conjugate continental margin of the present SCS would be north Palawan and Domain E. However, the conjugate continental margin of the Ryukyu continental margin is difficult to find, even if it is not a pre-requisite for the formation of the SCS marginal sea. Mindoro island is a piece of continental crust coming from the southeast, presently located in the eastern prolongation of the north Palawan continental domain. However, Mindoro cannot be considered as the conjugate margin of EU because Mindoro is moving with respect to EU since 18 Ma.

The last subducted domain of thinned continental crust is Domain A located north of S1 (Fig. 6). Its eastern boundary is defined until point **h** and it might eventually extend to point **a** on Fig. 6). Suppe et al. (2011) and Ustaszewski et al. (2012) suggest that when the HB-PSP oceanic lithosphere started to subduct beneath the Ryukyu margin, the Eurasian crust was delaminated with the lower part of the continental crust subducting with the slab and the upper part of the continental crust remaining fixed with respect to EU. Our model explains how the HB-PSP was able to subduct through the two lips of the tear fault T1 since ~18 Ma and why the delaminated continental crust bereaved of part of the lower crust was able to subduct beneath EU.

~20 Ma ago, ODP Site 1177 in the Shikoku basin and Site X28 on the northern SCS margin (Fig. 1) were at the same paleo-latitude (Liu et al., 2021). Zircon age spectra indicate that both sites were fed by materials from the Pearl river in the early Miocene (20 Ma), suggesting the Shikoku basin (eastern PSP) was dynamically linked

to the SCS in the early Miocene (Liu et al., 2021). In the middle Miocene (15 Ma), the Shikoku basin was separated from the SCS and received materials from the Yangtze river (Liu et al., 2021). ~20 Ma ago, our kinematic model (Fig. 10) and the bathymetric map of Fig. 1 show a decreasing depth path from Site X28 down to the SCS oceanic basin at 3000 m depth, then to the HB at more than 5000 m depth and then along the Ryukyu trench in direction of the Shikoku basin, avoiding the main topographic features in the vicinity of the Ryukyu trench as the Gagua ridge, Daito ridge and other elongated features. This decreasing depth path was favoring the sedimentary transit from the Pearl river to the Shikoku basin. 15 Ma ago, the intra-oceanic Luzon arc was already formed and subducting in the Ryukyu subduction zone with the upper part of the Luzon arc decoupled and possibly accreting along the Ryukyu sedimentary prism and forearc (Sibuet et al., 2004). We suggest the Luzon arc acted as a dam, interrupting the path of Pearl river sediments and favoring a new path from the Yangtze river.

~7 Ma ago, the two segments of EU margin south of Hualien (S2) and southwest of the northeastern SCS (S3) were still undeformed (Fig. 10C). The water depth of the adjacent SCS oceanic domain was close to the present water depth of the oceanic domain in the northwestern SCS, that is approximately 3 km. The Manila trench was bound to the east by the ~700-km long deep intra-oceanic Luzon arc (Fig. 10 C). At that time, the north Pacific subtropical gyre, flowing at the surface from tropics to higher latitudes in the North Pacific, was vigorously flowing into the SCS (Yin et al., 2021) above or through passages across the intra-oceanic deep Luzon arc chain (Fig. 10 C). Between ~7 and 6.5 Ma the Taiwan uplift and the accretion of the Luzon arc east of the LV occurred simultaneously with the uplift of the Bashi Strait, as shown by the bathymetry (Fig. 9). A semi-closure of the SCS was at the origin of a new oceanographic circulation regime in the latest Miocene with the isolation of the SCS from the North Pacific subtropical gyre (Yin et al., 2021). This topographic configuration induced a major shift in the paleo-circulation as shown by the two different contourite depositional systems identified west of Macclesfield bank, the deep one formed during the late Miocene by sediments transported from the north

Pacific ocean overlain by the latest Miocene to present sedimentary system issued from China or Taiwan (Yin et al., 2021).

4. Conclusions

The former extent and tectonic configuration of the subducted easternmost SCS, including the Eurasian COB, is established here from examining the present SCS, the Bashi Strait, the Ryukyu subduction zone, and by inference from seismic tomographic images of the Manila slab. Based on these constraints, we reconstruct a bayonet-shaped, stepped northern SCS COB that consists of a northeastern SCS COB segment we call 'S3', trending N070° that roughly parallels the present SCS shelf; a 350-km long ~N-S trending segment S2 that steps north to Hualien; and, a third segment S1 that extends from east of Hualien beneath the Ryukyu subduction zone trending N085° that ends near Miyako Island in the Ryukyus. The segment S1 is interpreted as a zone of weakness since ~18 Ma that ruptured as a tear fault from Miyako Island to east of Hualien. Subduction along the Manila transcurrent fault initiated ~18 Ma ago, creating the intra-oceanic Luzon arc, which began to collide ~7 Ma ago along the EU margin. From ~7 to 6.5 Ma Taiwan was uplifted west of the LV. The Luzon arc and forearc basins were shortened within the Coastal range. Our SCS-Taiwan reconstructions from ~18 Ma to Present show the main plate kinematics in terms of continental or oceanic nature of the main PSP-HB and EU entities before their subduction. These provide a new context for understanding regional tectonic events, including the Taiwan collision, regional sediment dispersion and paleo-ocean circulation.

Acknowledgments

This work was supported by National Natural Science Foundation of China (Grants 91958212 and 41730532) and Guangdong Natural Science Foundation research team project (Grant 2017A030312002). Jonny Wu was supported by US National Science Foundation Grant EAR-1848327. Scientific discussions with Mario Aurelio, Carla B. Dimalanta, Yu-Huan Hsieh, Chi-Yue Huang, Serge Lallemand, Jonathan C. Lewis, Andrew Lin, Jian Lin, Chuanzhou Liu, Char-Shine Liu, Karlo L.

Queaño, John Suppe, Brian Taylor and Mengming Yu are deeply acknowledged. Yu-Huan Hsieh, Chi-Yue Huang, Jonathan C. Lewis, Andrew Lin, Char-Shine Liu and Karlo L. Queaño kindly provided documents to understand critical problems or to draw some of the figures. Siqing Liu is acknowledged for his help to draw Supplementary Fig. S1. The pertinent and constructive reviews of Dieter Franke and of the Associate Editor Frédéric Mouthereau are particularly acknowledged. This paper is in memory of Tom Hilde who passed away in August 2020 and made important scientific contributions around Taiwan, in particular in the Philippine Sea and Okinawa trough. The GMT software (Wessel and Smith, 1995) was used to draw some of the figures.

References

Angelier, J. (1986). Geodynamics of the Eurasia Philippine Sea Plate boundary: Preface. Tectonophysics, 125(1–3), IX-X.

Angelier, J., F. Bergerat, H.-T. Chu, W. S. Juang and C.-Y. Lu (1990). Paleostress analysis as a key to margin extension: The Penghu Islands, South China Sea. Tectonophysics, 183, 161–176.

Angelier, J., H.-T. Chu and J.-C. Lee (1997). Shear concentration in a collision zone: Kinematics of the Chihshang fault as revealed by outcrop-scale quantification of active faulting, Longitudinal Valley, eastern Taiwan. Tectonophysics, 274, 117–143.

Arai, R., S. Kodaira, K. Yuka, T. Takahashi, S. Miura and Y. Kaneda (2017). Crustal structure of the southern Okinawa Trough: Symmetrical rifting, submarine volcano, and potential mantle accretion in the continental back-arc basin. J. Geophys. Res., 122, 622–641. doi:10.1002/2016JB013448.

Arcay, D., S. Lallemand, S. Abecassis and F. Garel (2020). Can subduction initiation at a transform fault be spontaneous? Solid Earth, 11, 37–62. doi:10.5194/se-11-37-2020.

Armada, L. T., S.-K. Hsu, C. B. Dimalanta, G. P. Yumul Jr, W.-B. Doo and Y.-C. Yeh (2020). Forearc structures and deformation along the Manila Trench. J. Asian Earth Sci., doi:10.1016/j.jaesx.2020.100036.

Armada, L. T., S.-K. Hsu, C.-Y. Ku, W.-N. Wu, C. Dimalanta and G. P. Yumul Jr

(2013). Possible northward extension of the Philippine Fault zone offshore Luzon Island (Philippines). Mar. Geophys. Res., 33, 369–377. DOI 10.1007/s11001-013-9169-5.

Aurelio, M. A., E. Barrier, R. Gaulon and C. Rangin (1997). Deformation stress states along the central segment of the Philippine Fault: Implications to wrench fault tectonics. J. Asian Earth Sci., 15, 107–119.

Barckhausen, U., M. Engels, D. Franke, S. Ladage and M. Pubellier (2014). Evolution of the South China Sea: Revised ages for breakup and seafloor spreading. Mar. Pet. Geol., 58, 599–611. doi:10.1016/j.marpetgeo.2014.02.022.

Bijwaard, H., W. Spakman and E. R. Engdahl (1998). Closing the gap between regional and global travel time topography. J. Geophys. Res., 103, 30055–30078.

Boutonnet, E., N. Arnaud, C. Guivel, Y. Lagabrielle, B. Scalabrino and F. Espinoza (2010). Subduction of the South Chile active spreading ridge: A 17 Ma to 3 Ma magmatic record in central Patagonia (western edge of Meseta del Lago Buenos Aires, Argentina). J. Volcanol. Geotherm. Res., 189(3-4), 319–339. doi:10.1016/j.jvolgeores.2009.11.022.

Briais, A., P. Patriat and P. Tapponnier (1993). Updated interpretation of magnetic anomalies and seafloor spreading stages in South China Sea: Implications for the Tertiary tectonics of Southeast Asia. J. Geophys. Res., 98, 6299–6328.

Brown, D., J. Alvarez-Marron, C. Biete, H. Kuo-Chen, G. Camanni and C.-W. Ho (2017). How the structural architecture of the Eurasian continental margin affects the structure, seismicity, and topography of the south central Taiwan fold-and-thrust belt. Tectonics, 36, 1275–1294. doi:10.1002/2017TC004475.

Canitano, A., M. Gordano and M. Y. Thomas (2021). Inherited state of stress as a key factor controlling slip and slip mode: Inference from the study of a slow slip event in the Longitudinal Valley, Taiwan. Geophys. Res. Lett., 48, e2020GL090278. doi:10.1029/2020GL090278.

Chi, W.-R. and J. Suppe (1985). Tectonic implications of Miocene sediments of Lan-Hsü Island, northern Luzon arc. Pet. Geol. Taiwan, 21, 93–106.

Conand, C., F. Mouthereau, J. Ganne, A. T. Lin, A. Lahfid, M. Daudet, L. Mesalles, S. Giletycz and M. Bonzani (2020). Strain partitioning and exhumation in oblique Taiwan collision: Role of rift architecture and plate kinematics. Tectonics, 38, doi:10.1029/2019TC005798.

Deschamps, A., P. Monié, S. E. Lallemand, S.-K. Hsu and K. Y. Yeh (2000). Evidence

for early Cretaceous oceanic crust trapped in the Philippine Sea plate. Earth Planet. Sci. Lett., 179, 503–516.

Eakin, D. H., K. D. McIntosh, H. J. A. Van Avendonk, L. Lavier, R. Lester, C.-S. Liu and C.-S. Lee (2014). Crustal-scale seismic profiles across the Manila subduction zone: The transition from intraoceanic subduction to incipient collision. J. Geophys. Res., 119, 1–17. doi:10.1002/2013JB010395.

Fisher, D. M., C.-Y. Lu and H.-T. Chu (2002). Taiwan Slate Belt: Insights into the ductile interior of an arc-continent collision. Geology and geophysics of an arc-continent collision, Taiwan. T. B. Byrne and C.-S. Liu, Geol. Soc. of America Special Paper. 358**,** 93–106.

Guan, Q.-S., T. Zhang, B. Taylor, J.-Y. Gao and J.-B. Li (2021). Ridge jump reorientation of the South China Sea revealed by high-resolution magnetic data. Terra Nova, DOI: 10.1111/ter.12532.

Hall, R. (2012). Late Jurassic-Cenozoic reconstructions of the Indonesian region and the Indian Ocean. Tectonophysics, 570–571, 1–41. doi:10.1016/j.tecto.2012.04.021.

He, L., K. Wang, L. Xiong and J. Wang (2001). Heat flow and thermal history of the South China Sea. Physics Earth and Planet. Int., 128(3–4), 211–220. DOI: 10.1016/S0031-9201(01)00256-4.

Hilde, T. W. C. and C.-S. Lee (1984). Origin and evolution of the west Philippine basin: A new interpretation. Tectonophysics, 102, 85–104.

Hirata, N., H. Kinoshita, H. Katao, H. Baba, Y. Kaiho, S. Koresawa, Y. Ono and K. Hayashi (1991). Report on DELP 1988 cruises in the Okinawa Trough. Part 3: Crustal structure of the southern Okinawa Trough. Bulletin of the Earthquake Research Institute, University of Tokyo, 66, 37–70.

Hsu, S.-K., Y.-C. Yeh, J.-C. Sibuet, W.-B. Doo and C.-H. Tsai (2013). A mega-splay fault system and tsunami hazard in the southern Ryukyu subduction zone. Earth and Planet. Sci. Lett., 362, 99–107. doi:10.1016/j.epsl.2012.11.053.

Huang, C.-Y., W.-H. Chen, M.-H. Wang, C.-T. Lin, S. Yang, X. Li, M. Yu, X. Zhao, K.-M. Yang, C.-S. Liu, Y.-H. Hsieh and R. Harrish (2018). Juxtaposed sequence stratigraphy, temporal-spatial variations of sedimentation and development of modern-forming forearc Lichi Mélange in North Luzon Trough forearc basin onshore and offshore eastern Taiwan: An overview. Earth-Science Reviews, 182, 102–140. doi:10.1016/j.earscirev.2018.01.015.

Huang, C.-Y., P. Wang, M. Yu, C.-F. You, C.-S. Liu, X. Zhao, L. Shao, G. Zhong and G. P. Yumul Jr. (2019). Potential role of strike-slip faults in opening up the South China Sea. National Science Review, 6, 891–901. doi:10.1093/nsr/nwz119.

Huang, C.-Y., P.-B. Yuan and S.-J. Tsao (2006). Temporal and spatial records of active arc-continent collision in Taiwan: A synthesis. Geol. Soc. Am. Bull., 118, 274–288. doi:10.1130/B25527.1.

Jolivet, L. and J.-P. Brun (2010). Cenozoic geodynamic evolution of the Aegean. Int. J. Earth Sci., 99, 109–138.

Klingelhoefer, F., T. Berthet, S. Lallemand, P. Schnurle, C.-S. Lee, C.-S. Liu, K. McIntosh and T. Theunissen (2012). P-wave velocity structure of the southern Ryukyu margin east of Taiwan: Results from the ACTS wide-angle seismic experiment. Tectonophysics, 578, 50–62. doi:10.1016/j.tecto.2011.10.010.

Lallemand, S., Y. Font, H. Bijwaard and H. Kao (2001). New insights on 3-D plates interaction near Taiwan from tomography and tectonic implications. Tectonophysics, 335, 229–253.

Lallemand, S., C.-S. Liu, S. Dominguez, P. Schnürle, J. Malavieille and the ACT scientific crew (1999). Trench-parallel stretching and folding of forearc basins and lateral migration of the accretionnary wedge in the southern Ryukyus: A cause of strain partition caused by oblique convergence. Tectonics, 18, 231–247.

Lallemand, S., C.-S. Liu and Y. Font (1997). A tear fault boundary between the Taiwan orogen and the Ryukyu subduction zone. Tectonophysics, 274, 171–190.

Lallemand, S. and H.-H. Tsien (1997). An introduction to active collision in Taiwan. Tectonophysics, 274, 1–4.

Lee, C.-S., J. Shor, G.G., L. D. Bibee, R. S. Lu and T. Hilde (1980). Okinawa Trough: Origin of a back-arc basin. Mar. Geol., 35, 219–241.

Lee, J.-C., J. Angelier and H.-T. Chu (1997). Polyphase history and kinematics of a complex major fault zone in the northern Taiwan mountain belt: The Lishan fault. Tectonophysics, 274, 97–115.

Lee, Y.-H., T. Byrne, W.-H. Wang, W. Lo, R.-J. Rau and H.-Y. Lu (2015). Simultaneous mountain building in the Taiwan orogenic belt. Geology, 43, 451–454. doi:10.1130/G36373.1.

Lester, R., K. McIntosh, H. J. A. Van Avendonk, L. Lavier, C.-S. Liu and T. K. Wang

(2013). Crustal accretion in the Manila trench accretionary wedge at the transition from subduction to mountain-building in Taiwan. Earth Planet. Sci. Lett., 375, 430–440.

Lester, R., H. J. A. Van Avendonk, K. McIntosh, L. Lavier, C.-S. Liu, T.-K. Wang and F. Wu (2014). Rifting and magmatism in the northeastern South China Sea from wide-angle tomography and seismic reflection imaging. J. Geophys. Res., 119, 2305–2323. doi:10.1002/2013JB010639.

Lester, W. R., L. Lavier, K. D. McIntosh, H. J. A. Van Avendonk and F. Wu (2012). Active extension in Taiwan's precollision zone: A new model of plate bending in continental crust. Geology, 40(9), 2437–2440. doi: 10.1130/G33142.1.

Lewis, J. C., D. J. O'Hara and R.-J. Rau (2015). Seismogenic strain across the transition from fore-arc slivering to collision in southern Taiwan. J. Geophys. Res., 120, doi:10.1002/ 2015JB011906.

Li, C., R. D. van der Hilst, E. R. Engdahl and S. Burdick (2008). A new global model for P wave speed variations in Earth's mantle. Geochem. Geophys. Geosyst., 9(8), doi:10.1029/2007GC001806.

Lin, A. T. and A. B. Watts (2002). Origin of the west Taiwan basin by orogenic loading and flexure of a rifted continental margin. J. Geophys. Res., 107, 2185. doi:10.1029/2001JB000669.

Lin, A. T., A. B. Watts and S. P. Hesselbo (2003). Cenozoic stratigraphy and subsidence history of the South China Sea margin in the Taiwan region. Basin Research, 15, 453–478.

Liu, C.-S., P. Schnurle, S. Lallemand and D. L. Reed (1997). TAICRUST and deep seismic imaging of western end of Ryukyu Arc-Trench system. JAMSTEC Journal of Deep Sea Res., Special Volume, 39–45.

Liu, S., M. H. Zhao, J.-C. Sibuet, X. Qiu, J. Wu, J. Zhang, C. Chen, Y. Xu and L. Sun (2018). Geophysical constraints on the lithospheric structure in the northeastern South China Sea and its implications for the South China Sea geodynamics. Tectonophysics, 742-743, 101–119. doi:10.1016/j.tecto.2018.06.002.

Liu, W., C. Gai, W. Feng, W. Cao, L. Guo, Y. Zhong, J. Liu, Y. Zhou, Y.-M. Chou, J. Lin and Q. Liu (2021). Coeval Evolution of the Eastern Philippine Sea Plate and the South China Sea in the Early Miocene: Paleomagnetic and Provenance Constraints From ODP Site 1177. Geophys. Res. Lett., 48, e2021GL093916. doi:10.1029/2021GL093916.

McIntosh, K., L. Lavier, H. van Avendonk, R. Lester, D. Eakin and C.-S. Liu (2014). Crustal structure and inferred rifting processes in the northeast South China Sea. Mar. Pet. Geol., 58, 612–626. doi:10.1016/j.marpetgeo.2014.03.012.

McIntosh, K., H. van Avendonk, L. Lavier, W. R. Lester, D. Eakin, F. Wu, C.-S. Liu and C.-S. Lee (2013). Inversion of a hyper-extended rifted margin in the southern Central Range of Taiwan. Geology, 41, 871–874. doi:10.1130/G34402.1.

Mesalles, L., F. Mouthereau, M. Bernet, C.-P. Chang, A. T. Lin, C. Fillon and X. Sengelen (2014). From submarine continental accretion to arc-continent orogenic evolution: The thermal record in southern Taiwan. Geology, 42, 907–910. doi:10.1130/G35854.1.

Miki, M. (1995). Two-phase opening model for the Okinawa Trough inferred from paleomagnetic study of the Ryukyu arc. J. Geophys. Res., 100, 8169–8184.

Misawa, A., M. Sato, S. Furuyama, J. H. Chang, T. Inoue and K. Arai (2020). Embryonic rifting zone revealed by a high-density survey on the southern margin of the southern Okinawa Trough. Geophys. Res. Lett., 47, doi:10.1029/2020GL090161.

Nayak, K., A. T. Lin, K.-F. Huang, Z. Liu, N. Babonneau, G. Ratzov, R. K. Pillutla, P. Das and S.-K. Hsu (2021). Clay-mineral distribution in recent deep-sea sediments around Taiwan: Implications for sediment dispersal processes. Tectonophysics, 814, 228974. doi:10.1016/j.tecto.2021.228974.

Nissen, S. S., D. E. Hayes, P. Buhl, J. Diebold, Y. Bochu, Z. Weijun and C. Yongqin (1995). Deep penetration seismic soundings across the northern margin of the South China Sea. J. Geophys. Res., 100, 22,407–422,433.

Özbakır, A. D., R. Govers and A. Fichtner (2020). The Kefalonia Transform Fault: A STEP fault in the making. Tectonophysics, 787, 228471. doi:10.1016/j.tecto.2020.228471.

Pan, T.-Y., A. T. Lin and W.-R. Chi (2015). Paleoenvironments of the evolving Pliocene to early Pleistocene foreland basin in northwestern Taiwan: An example from the Dahan River section. Island Arc, 24, 317–341.

Pautot, G., C. Rangin, A. Briais, P. Tapponnier, P. Beuzart, G. Lericolais, X. Mathieu, J. Wu, S. Han, H. Li, Y. Lu and J. Zhao (1986). Spreading direction in the central South China Sea. Nature, 321, 150–154.

Pautot, G., C. Rangin, A. Briais, J. Wu, S. Han, H. Li, Y. Lu and J. Zhao (1990). The axial ridge of the South China Sea: A Seabeam and geophysical Geodynamics

survey. Oceanologica Acta, 13(2), 129–143.

Qian, S., X. Zhang, J. Wu, S. Lallemand, A. R. L. Nichols, C.-Y. Huang, D. P. Miggins and H. Zhou (2021). First identification of a Cathaysian continental fragment beneath the Gagua Ridge, Philippine Sea, and its tectonic implications. Geology, doi:10.1130/G48956.1.

Queaño, K. L., J. R. Ali, J. Milsom, J. C. Aitchison and M. Pubellier (2007). North Luzon and the Philippine Sea Plate motion model: Insights following paleomagnetic, structural, and age-dating investigations. J. Geophys. Res., 112, B05101. doi:10.1029/2006JB004506.

Richard, M., H. Bellon, R. C. Maury, E. Barrier and W.-S. Jiang (1986). Miocene to Recent calc-alkalic volcanism in eastern Taiwan: K-Ar ages and petrography. Tectonophysics, 125, 87–102.

Seno, T. (1977). The instantaneous rotation vector of the Philippine Sea plate relative to the Eurasian plate. Tectonophysics, 42, 209–226.

Shao, W.-Y., S.-L. Chung, W.-S. Chen, H. Y. Lee and L.-W. Xie (2015). Old continental zircons from a young oceanic arc, eastern Taiwan: Implications for Luzon subduction initiation and Asian accretionary orogeny. Geology, 43, 479–482. doi:10.1130/G36499.1.

Shinjo, R. (1999). Geochemistry of high Mg andesites and the tectonic evolution of the Okinawa Trough - Ryukyu arc system. Chemical Geology, 157, 69–88.

Shinjo, R., S.-L. Chung, N. Kato and M. Kimura (1999). Geochemical and Sr-Nd isotopic characteristics of volcanic rocks from the Okinawa Trough and Ryukyu arc: Implications for the evolution of a young, intra-continental back arc basin. J. Geophys. Res., 104, 10,591–10,608.

Sibuet, J.-C., S.-K. Hsu and E. Debayle (2004). Geodynamic context of the Taiwan orogen. Continent-Ocean Interactions Within East Asian Marginal Seas. P. Clift, P. Wang, W. Kuhnt and D. E. Hayes, American Geophysical Union monograph, Washington, D.C. 149, 127–158.

Sibuet, J.-C., S.-K. Hsu, C.-T. Shyu and C.-S. Liu (1995). Structural and kinematic evolution of the Okinawa trough backarc basin. Backarc Basins: Tectonics and Magmatism. B. Taylor. New York, Plenum Press**,** 343–378.

Sibuet, J.-C., J. Letouzey, F. Barbier, J. Charvet, J.-P. Foucher, T. W. C. Hilde, M. Kimura, L.-Y. Chiao, B. Marsset, C. Muller and J.-F. Stéphan (1987). Backarc extension in the Okinawa Trough. J. Geophys. Res., 92, 14041–14063.

Sibuet, J.-C., Y. Thomas, B. Marsset, H. Nouzé, V. Louvel, B. Savoye and J.-P. Le Formal (1996). Detailed relationship between tectonics and sedimentation from Pasisar deep-tow seismic data acquired in the Iberia Abyssal Plain Proceedings of the Ocean Drilling Program, Scientific Results. R. B. Whitmarsh, D. S. Sawyer, A. Klaus and D. G. Masson. College Station, TX Ocean Drilling Program. 149, 649–657.

Sibuet, J.-C., Y.-C. Yeh and C.-S. Lee (2016). Geodynamics of the South China Sea. Tectonophysics, 692, 98–119. doi:10.1016/j.tecto.2016.02.022.

Simoes, M., J.-P. Avouac, O. Beyssac, B. Goffe, K. A. Farley and Y.-G. Chen (2007). Mountain building in Taiwan: A thermokinematic model. J. Geophys. Res., 112, B11405. doi:10.1029/2006JB004824.

Sisson, V. B., T. L. Pavlis, S. M. Roeske and D. J. Thorkelson (2003). Introduction: An overview of ridge-trench interactions in modern and ancient settings. Geology of a transpressional orogen developed during ridge-trench interaction along the North Pacific margin. V. B. Sisson, S. M. Roeske and T. L. Pavlis. Boulder, Colorado, Geological Society of America Special Paper. 371, 1–18.

Spakman, W. and R. Hall (2010). Surface deformation and slab-mantle interaction during Banda arc subduction rollback. Nature Geoscience, 3, 562–566. DOI: 10.1038/NGEO917.

Suppe, J. (1981). Mechanics of mountain building and metamorphism in Taiwan. Geol. Soc. of China, 4, 67–89.

Suppe, J., S. Carena, Y.-M. Wu and K. Ustaszewski (2011). Subducted lithosphere, slab tearing and continental delamination under Taiwan: arc-continent collision at the junction of quasi-orthogonal subduction systems. AGU Fall Meeting 2011 Abstract, San Francisco, USA.

Taylor, B., A. M. Goodliffe and F. Martinez (1999). How continents break up: Insights from Papua New Guinea. J. Geophys. Res., 104, 7497–7512.

Teng, L. S. (1990). Geotectonic evolution of late Cenozoic arc-continent collision in Taiwan. Tectonophysics, 183, 57–76.

Teng, L. S., Y. Wang, C. H. Tang, T. C. Huang, M. S. Yu and A. Ke (1991). Tectonic aspects of the Paleogene deposition basin of northern Taiwan. Geol. Soc. of China, 34, 313–336.

Tsai, C.-H., J. B. H. Shyu, S.-L. Chung and H.-Y. Lee (2020). Miocene sedimentary provenance and paleogeography of the Hengchun Peninsula, southern Taiwan:

Implications for tectonic development of the Taiwan orogen. J. Asian Earth Sci., 194, 104032. doi:10.1016/j.jseaes.2019.104032.

Ustaszewski, K., Y.-M. Wu, J. Suppe, H.-H. Huang, C.-H. Chang and S. Carena (2012). Crust–mantle boundaries in the Taiwan–Luzon arc-continent collision system determined from local earthquake tomography and 1D models: Implications for the mode of subduction polarity reversal. Tectonophysics, 578, 31–49. doi:10.1016/j.tecto.2011.12.029.

Van Avendonk, H. J. A., K. D. McIntosh, H. Kuo-Chen, L. L. Lavier, D. A. Okaya, F. T. Wu, C. Y. Wang, C.-S. Lee and C.-S. Liu (2016). A lithospheric profile across northern Taiwan: from arc-continent collision to extension. Geophys. J. Int., 204, 331–346. doi: 10.1093/gji/ggv468.

Wan, X., C. F. Li, M. Zhao, E. He, S. Liu, X. Qiu, Y. Lu and N. Chen (2019). Seismic velocity structure of the magnetic quiet zone and continent-ocean boundary in the northeastern South China Sea. J. Geophys. Res., 124, 11,866-11,899. doi:10.1029/2019JB017785.

Wang, T.-K., M.-K. Chen, C.-S. Lee and K. Xia (2006). Seismic imaging of the transitional crust across the northeastern margin of the South China Sea. Tectonophysics, 412, 237–254. doi:10.1016/j.tecto.2005.10.039.

Wang, T.-K., K. McIntosh, Y. Nakamura, C.-S. Liu and H.-W. Chen (2001). Velocity-interface structure of the southwestern Ryukyu subduction zone from EW9509-1 OBS/MCS data. Mar. Geophys. Res., 22, 265–287.

Wernicke, B. (1985). Uniform-sense normal simple shear of the continental lithosphere. Canadian J. Earth Sci., 22(1), 108–125. DOI: 10.1139/e85-009.

Wessel, P. and W. H. F. Smith (1995). New version of the generic mapping tools released. Eos. Trans. AGU, 76, 329.

Wu, J. and J. Suppe (2018). Proto-South China Sea plate tectonics using subducted slab constraints from tomography. J. of Earth Sci., 29(6), 1304–1318. doi:10.1007/s12583-017-0813-x.

Wu, J., J. Suppe, R. Lu and R. Kanda (2016). Philippine Sea and East Asian plate tectonics since 52 Ma constrained by new subducted slab reconstruction methods. J. Geophys. Res., 121, 4670–4741. doi:10.1002/2016JB012923.

Yeh, Y.-C., S.-K. Hsu, W.-B. Doo, J.-C. Sibuet, C.-S. Liu and C.-S. Lee (2012). Crustal features of the northeastern South China Sea: Insights from seismic and magnetic interpretations. Mar. Geophys. Res., 33, 3307-326.

doi:10.1007/s11001-012-9154-4.

Yin, S., F. J. Hernández‐Molina, L. Lin, J. X. Chen, W. F. Ding and J. B. Li (2021). Isolation of the South China Sea from the North Pacific Subtropical Gyre since the latest Miocene due to formation of the Luzon Strait. Scientific Reports, doi:10.1038/s41598-020-79941-4.

Yu, S.-B. and L.-C. Kuo (2001). Present-day crustal motion along the Longitudinal Valley Fault, eastern Taiwan. Tectonophysics, 333, 199–217.

Yu, S.-B., L.-C. Kuo, R. S. Punongbayan and E. G. Ramos (1999). GPS observation of crustal deformation in the Taiwan-Luzon region. Geophys. Res. Lett., 26, 923–926.

Zhao, M.-H., E. He, J.-C. Sibuet, L. Sun, X. Qiu, P. Tan and J. Wang (2018). Postseafloor spreading volcanism in the central east South China Sea and its formation through an extremely thin oceanic crust. Geochem. Geophys. Geosyst., 19, 621-641. doi:10.1002/2017GC007034.

Zhao, M. H., J.-C. Sibuet and J. Wu (2019). Intermingled fates of South China Sea and Philippine Sea plate. National Science Review, 6, 886–890. doi:10.1093/nsr/nwz107.

Zhao, X., C.-Y. Huang, H. Ren, J. Guo, W. Chen and W. Yuan (2016). Paleomagnetic evidence of clockwise rotation of the Lanyu Island of SE Taiwan since the Late Pliocene. Fall AGU meeting abstract OS51C-2075, San Francisco, California.

Credit Author Statement

J.-C. S. developed the idea and wrote the paper. M. Z. did some of the figures and wrote part of the paper. J. W. calculated synthetic plate reconstruction and improved the paper. C.-S. L. provided swath-bathymetry map and participated in the interpretation.

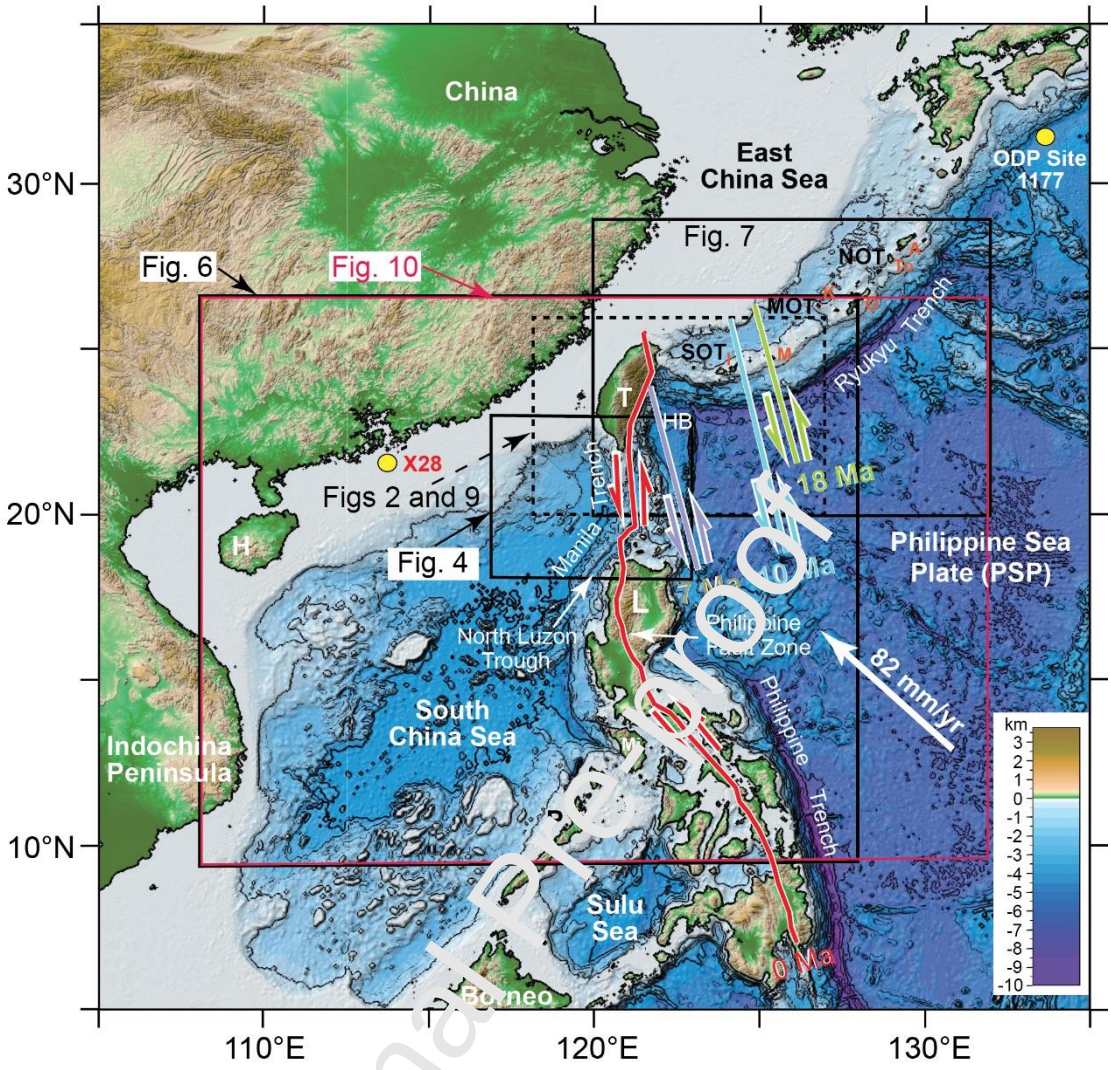

Fig. 1 (Sibuet et al., 2021, revised Tectonophysics)

Fig. 1 Bathymetric map of SE Asia with HB-PSP/EU shear plate boundaries at ~18, 10, ~7 Ma and Present. For clarity, only the present HB-PSP/EU shear plate boundary extends to the south. The rectangles are locations of figures shown in the text. A, Amami Island; EU, Eurasian plate; H, Hainan; HB, Huatung basin; I, Ishigaki Island; K, Kume Island; L, Luzon Island; M, Miyako Island; Mi, Mindoro Island; MOT, middle Okinawa trough; NOT, northern Okinawa trough; P, Palawan; PSP, Philippine Sea plate; SOT, southern Okinawa trough; T, Taiwan Island; To, Tokuno Island. Drilling sites ODP 1177 in the Sikoku basin and X28 offshore the Guangdong province (Liu et al., 2021) are shown.

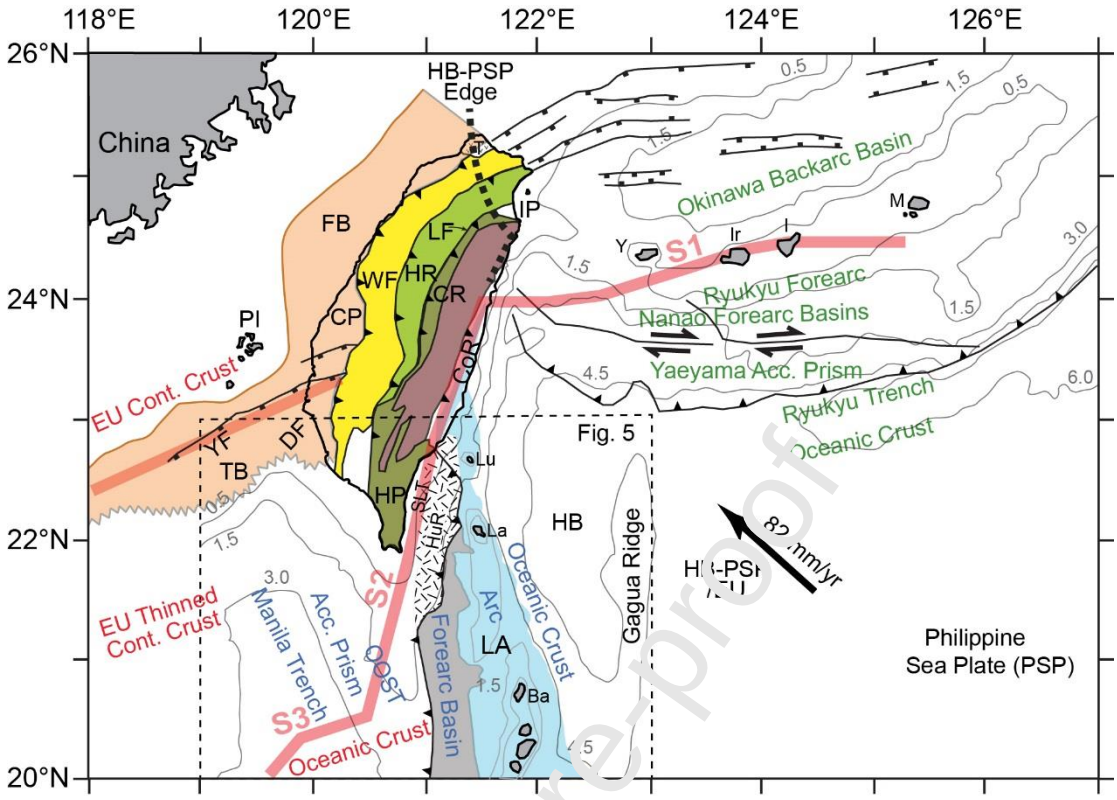

Fig. 2 (Sibuet et al., 2021, revised Tectonophysics)

Fig. 2 Main geological features in the Taiwan region and boundaries of main domains. Written in red: features of northeastern SCS margin with the hinge line following the Yichu fault in pink; in blue: features of Manila subduction zone; in green: features of Ryukyu subduction zone. Present-day isobaths in grey every 1.5 km plus isobath 0.5 km. S1, S2 and S3 are segments of continent-ocean boundaries (COB) established from tomographic data (Wu et al., 2016) of the Manila slab. Ba, Batan Island; CoR, Coastal range; CP, Coastal plain; CR, Central range; DF, Deformation front; EU, Eurasian plate; FB, Foreland basin; HB, Huatung basin; HP, Hengchun peninsula; HR, Hsuehshan range; HuR, Huatung ridge; I, Ishigaki Island; IP, Ilan plain; Ir, Iriomote Island; La, Lanyu Island; LA, Luzon arc; LF, Lishan fault; Lu, Lutao Island; M, Miyako Island; OOST; out-of-sequence thrust; PI, Penghu Islands; PSP, Philippine Sea plate; SLT, southern Longitudinal trough; T, Tatun volcano; TB, Tainan basin; WF, Western foothills; Y, Yonaguni Island; YF, Yichu fault.

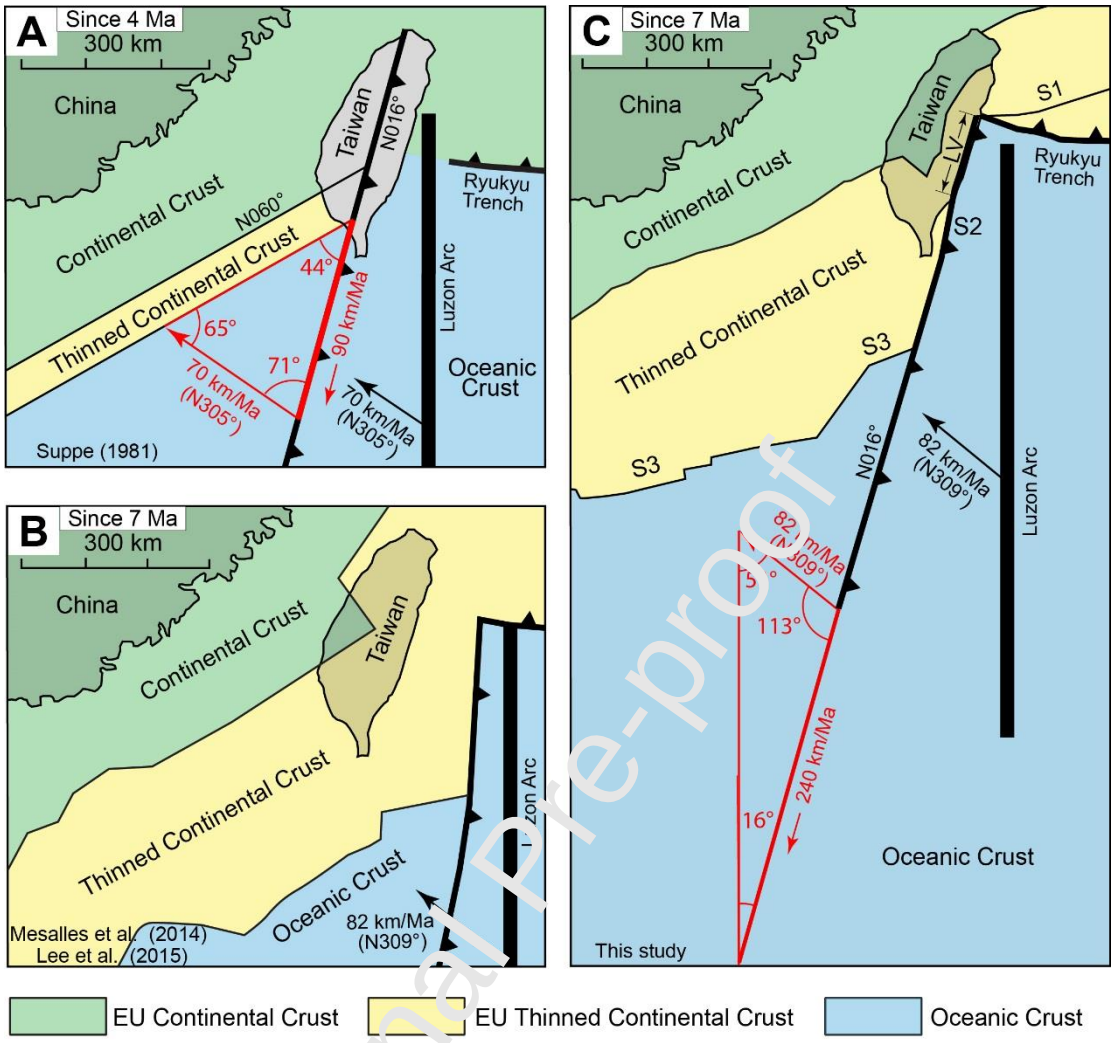

Fig. 3 (Sibuet et al., 2021, revised Tectonophysics)

Fig. 3 Velocity triangles for the Luzon arc-continent collision in Taiwan. A) Sketch from Suppe (1981). B) Sketch from Mesalles et al. (2014) and Lee et al. (2015) where the Luzon arc is parallel to the N-S oriented COB. C) Sketch from this study where collision propagates ~3 times faster to the south than in Suppe sketch. LV, Longitudinal valley; S1, S2 and S3 are SCS northern COB segments.

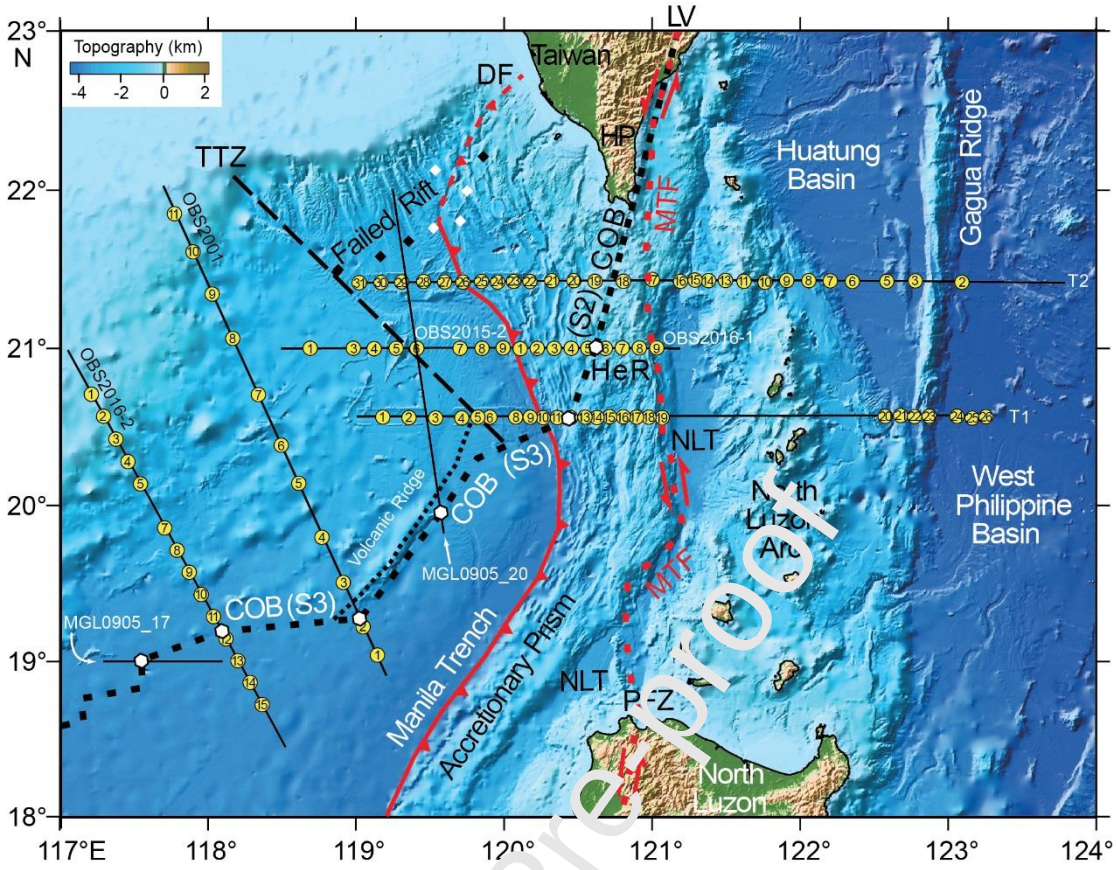

Fig. 4 (Sibuet et al., 2021, revised Tectonophysics)

Fig. 4 Identification of the northern SCS continent-ocean boundary (COB) and of the present Manila transcurrent fault (MTF) initiated ~18 Ma ago. North of 19°N, the accretionary prism is located between the Manila trench and the MTF. The trace of the COB along segment S3 is shown by white hexagons along MCS profiles MGL0905-17 and 20, and refraction profiles OBS2016-2, OBS2001, T1 and OBS2016-1. The trace of the COB along the southern part of segment S2 is identified on refraction profiles T1 and OBS2016-1 (white hexagons) but not further north. North of 21°N, the location of S2 (dashed line with closely spaced hyphens) corresponds to the present location of S2, which merged with the MTF. The location of the initial COB was perhaps a few tens kilometers further east. DF, Deformation front; HeR, Hengchun ridge; HP, Hengchun peninsula; NLT, North Luzon trough; PFZ, Philippine Fault zone.

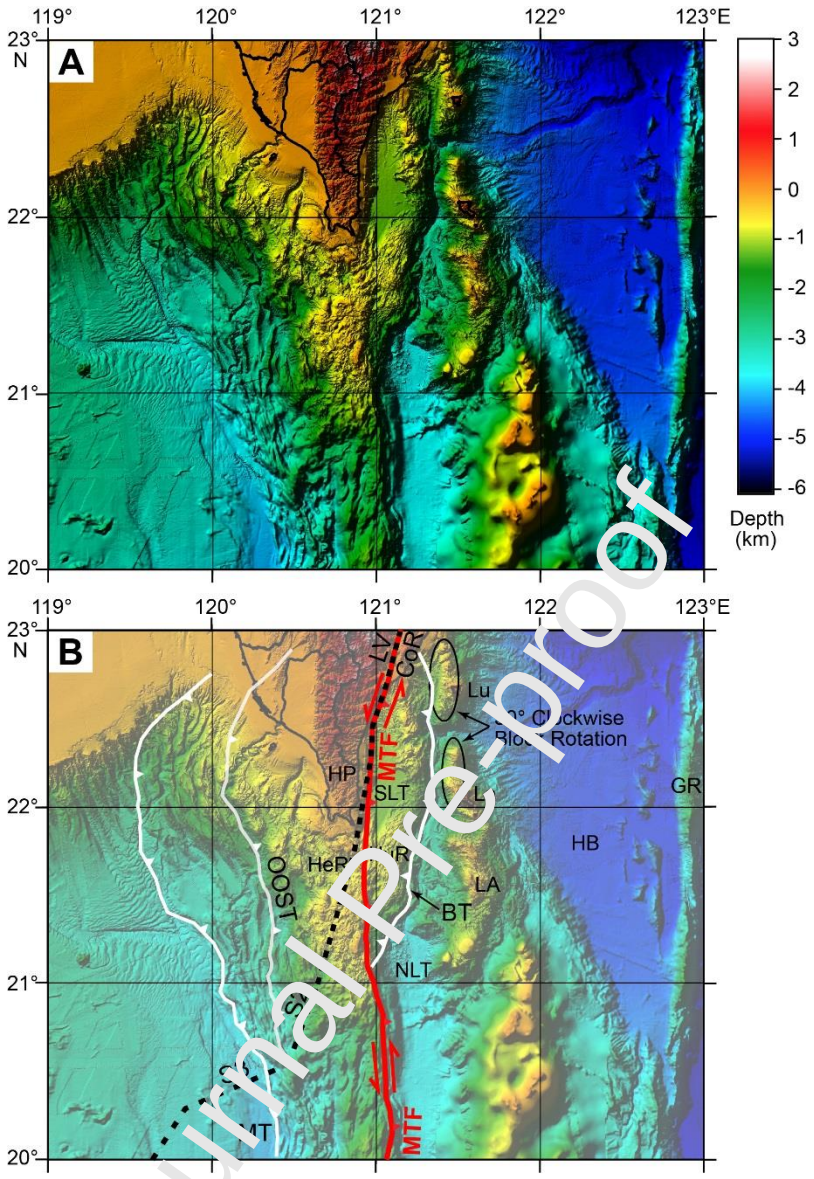

Fig. 5 (Sibuet et al., 2021, revised Tectonophysics)

Fig. 5 Bathymetric map of the Bashi Strait including available swath-bathymetric data with illumination from the NW. A) Original figure with color bar for topography. B) Interpretation of the document showing the location of S2, S3 and the present left-lateral Manila transcurrent shear fault (MTF, red continuous line). Thrust faults in white with triangles. BT, Back thrust; CoR, Coastal range; HB, Huatung basin; HeR, Hengchun ridge; HP, Hengchun peninsula; HuR, Huatung ridge; La, Lanyu Island; LA, Luzon arc; Lu, Lutao Island; LV, Longitudinal valley; MT, Manila trench; NLT, north Luzon trough; OOST; out-of-sequence thrust; PSP, Philippine Sea plate; SLT, southern Longitudinal trough.

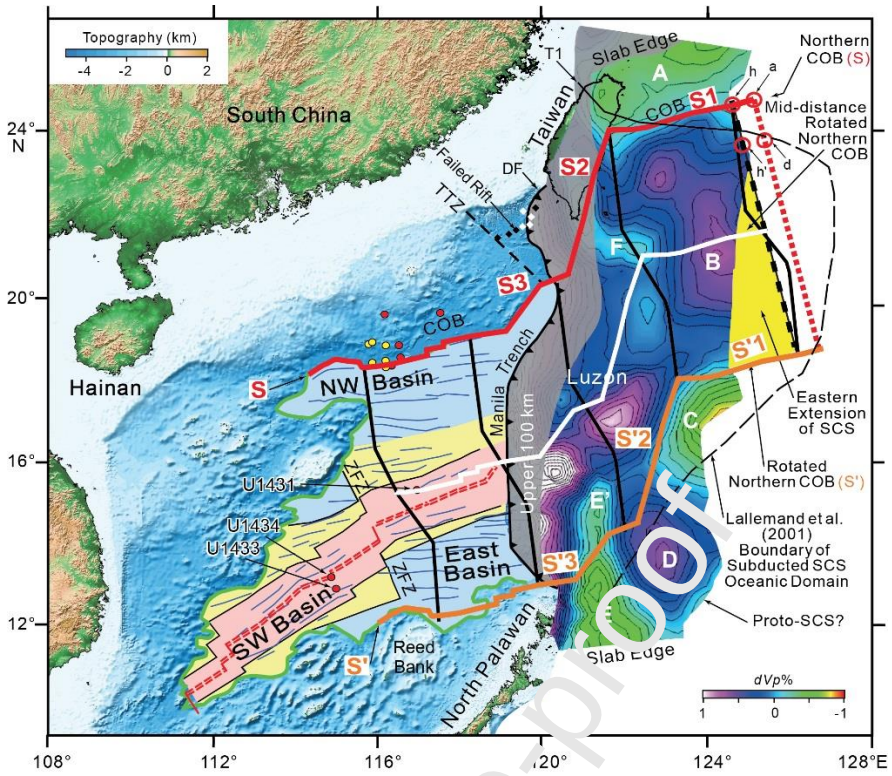

Fig. 6 (Sibuet et al., 2021, revised Tectonophysics)

Fig. 6 South China Sea (SCS) oceanic domain and unfolded Manila slab. The unfolded Manila slab is colored by its intra-slab tomographic velocities *dVp* (Wu et al., 2016) and is attached to the SCS along the Manila trench. The N-S grey shadow mask (<100 km width) corresponds to probable artifacts and was not interpreted. Seafloor spreading flow-lines in black are from Sibuet et al. (2016). The northern COB rotated with respect to Eurasia (EU) (in orange) follows the observed southern COB (green line). The mid-distance rotated northern COB (in white) follows the extinct spreading ridge located in the present SCS. S1, S2 and S3 are northern COB segments and S'1, S'2 and S'3 are southern COB segments. The yellow area is the suggested eastern extension of the Manila slab oceanic domain discussed in the text. Points **a, d, h** and **h'** also appear in Fig. 7. Starting from point **a**, the dashed red line between S1 and S'1 is the assumed eastern limit of the Manila slab. The dashed thin black line is the boundary of the SCS oceanic domain by Lallemand et al. (2001), which continues to the west as a continuous thin black line interpreted as tear fault T1 (Lallemand et al., 2001). Areas A, B, C, D, E, E' and F are discussed in the text. The yellow and red dots are the drilling sites of the International Ocean Drilling Program. DF, Deformation front; TTZ, Taiwan transfer Zone; ZFZ, Zhongnan fracture zone.

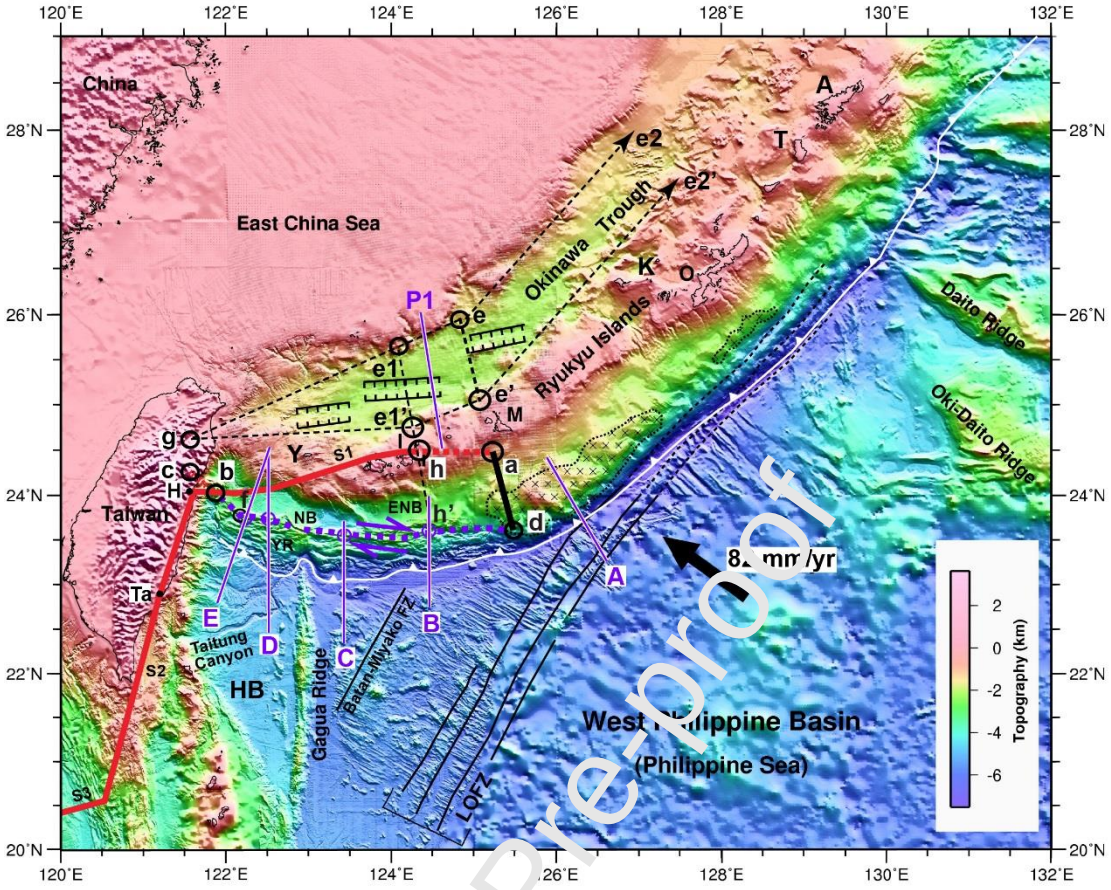

Fig. 7 (Sibuet et al., 2021, revised Tectonophysics)

Fig. 7 Bathymetric map including swath-bathymetric data (Hsu et al., 2013) showing the location of the continent-ocean boundary (COB) S1 before (red line) and after (purple dashed line) the opening of the Okinawa trough (OT). S1, S2 and S3 are northern COB segments (continuous red line prolonged by a dashed red line between points **h** and **a**). The purple dashed line (**dh'fb**) located at the rear of the Yaeyama ridge (YR) is the present COB location. Line **ad** (thick black line) corresponds to a portion of the SCS eastern boundary defined in Fig. 6. The two black dashed lines starting from point **g** at the OT western tip give the OT extension. A, Amami Island; ENB, east Nanao basin; H, Hualien city; HB, Huatung basin; I, Ishigaki Island; K, Kume Island; M, Miyako Island; NB, Nanao basin; O, Okinawa Island; T, Tokuno Island; Ta, Taitung city; Y, Yonaguni Island.

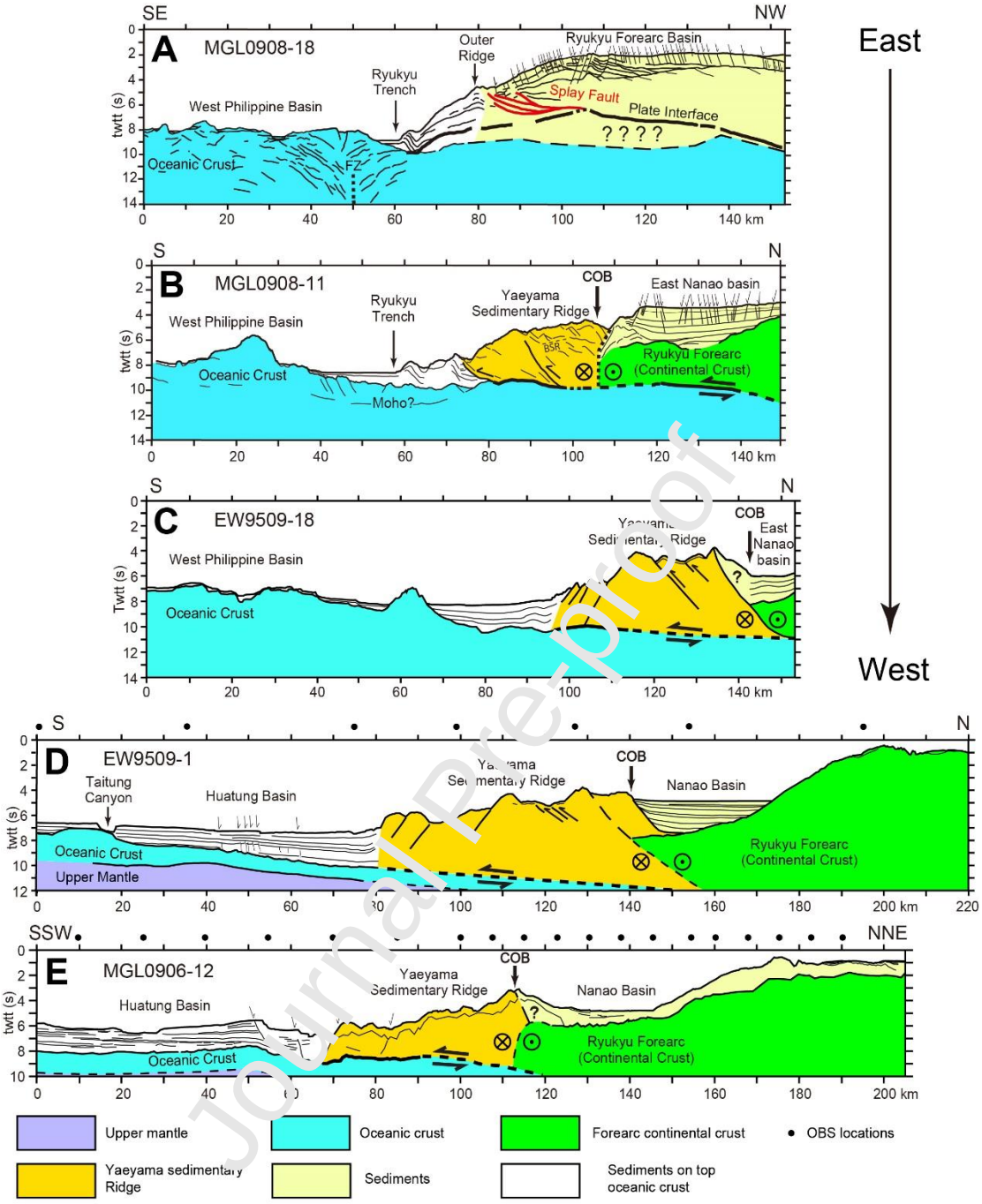

Fig. 8 (Sibuet et al., 2021, revised Tectonophysics)

Fig. 8 Line drawings of deep seismic profiles shot across the lower part of the Ryukyu subduction zone. Profiles A to E are located in Fig. 7. Wide-angle reflection and refraction data were collected along profiles D and E. In the absence of refraction data, the Moho is not imaged in Profiles A to C.

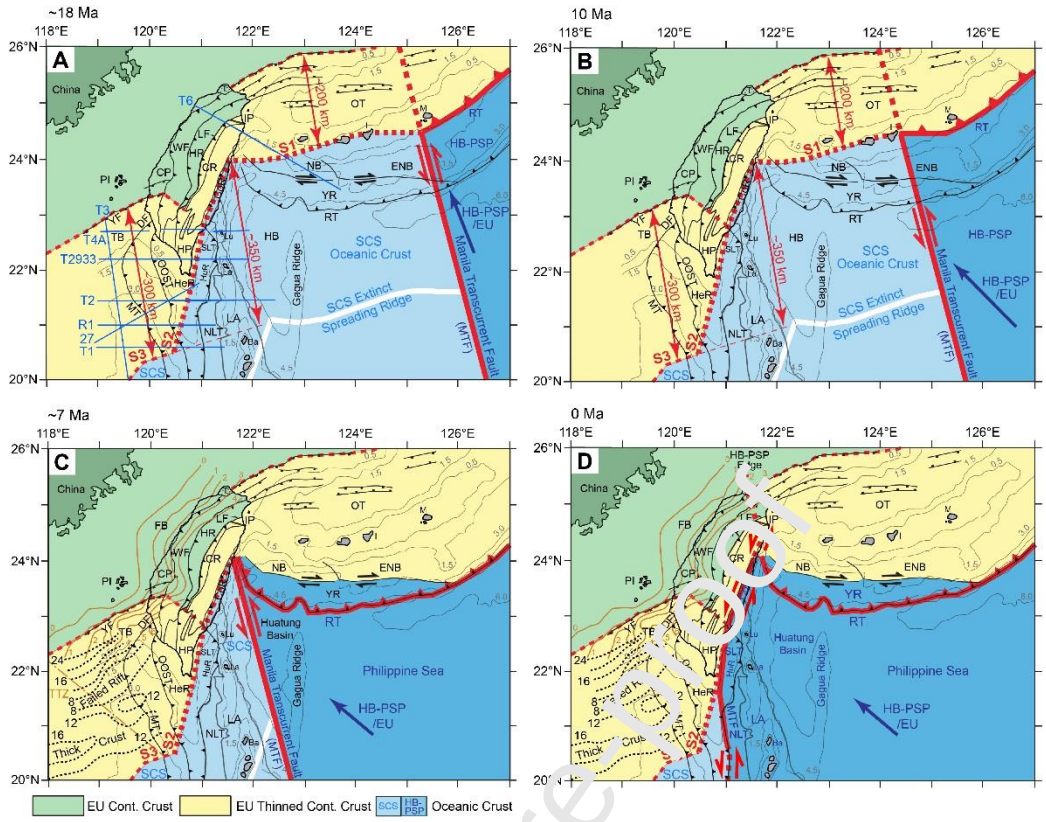

Fig. 9 (Sibuet et al., 2021, revised Tectonophysics)

Fig. 9 Kinematic evolution ~18 Ma ago, at the time of the initiation of the Manila transcurrent fault and of the tear of the Eurasian plate (Fig. 9A), 10 Ma ago at the time of the onset of OT opening and beginning of Ryukyu arc rotation (Fig. 9B), ~7 Ma ago at the time of the beginning of Luzon arc collision with EU (Fig. 9C), and today. All features represent present-day features, and are the same on the four panels: EU continental (in light green) and thinned continental crusts (in yellow); SCS oceanic crust (light blue), and Huatung basin-Philippine Sea plate (HB-PSP) oceanic crust (dark blue); SCS extinct spreading ridge (white line); active plate boundaries (continuous thick red lines) around the HB-PSP oceanic domain; HB-PSP/EU motion from one stage to the following more recent stage (dark blue arrows); present-day isobaths every 1.5 km plus isobath 0.5 km; northern COB segments (S1, S2 and S3). Ba, Batan Island; CoR, Coastal range; CP, Coastal plain; CR, Central range; DF, Deformation front; ENB, east Nanao basin; HP, Hengchun peninsula; HR, Hsuehshan range; HuR, Huatung ridge; I, Ishigaki Island; IP, Ilan plain; Ir, Iriomote Island; La, Lanyu Island; LA, Luzon arc; LF, Lishan fault; Lu, Lutao Island; M, Miyako Island; MT, Manila trench; NB, MTF, Manila transcurrent fault; Nanao basin; NLT, north Luzon trough; OOST; out-of-sequence thrust; OT, Okinawa trough; PI, Penghu Islands; SLT, southern Longitudinal trough; T, Tatun volcano; TB, Tainan basin; WF, Western foothills; Y, Yonaguni Island; YF, Yichu

fault; YR, Yaeyama ridge.

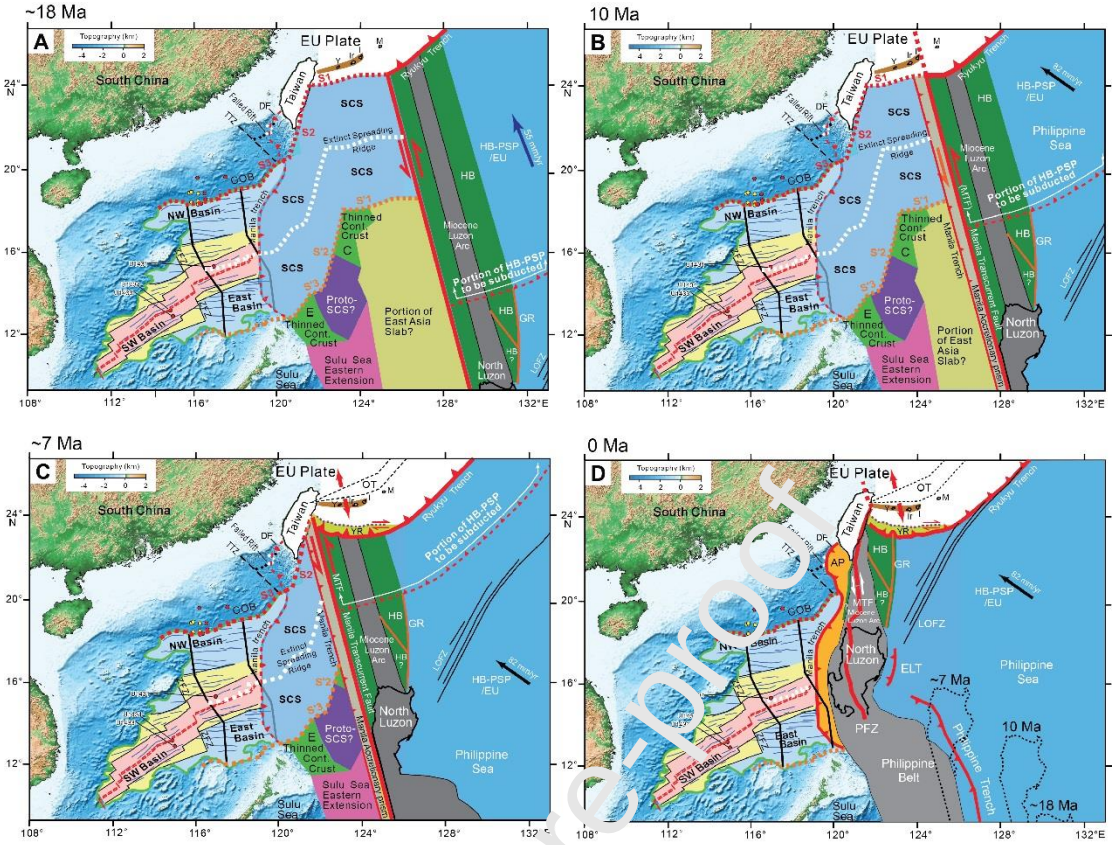

Fig. 10 (Sibuet et al., 2021, revised Tectonophysics)

Fig. 10 Kinematic reconstructions at ~18 Ma, 10 Ma, ~7 Ma and Present (Figs. A to D) with regions of oceanic or thinned continental crust interpreted from Manila slab tomographic data of Fig. 6 and present-day SCS oceanic regions with seafloor spreading flow-lines (Sibuet et al., 2016). In each panel, continuous red lines are active features from this panel to the next one. In the subducted SCS, areas C and D are two thinned continental regions (in green) surrounded by oceanic crust, which constrain the geodynamic evolution of Taiwan and of the Gagua ridge. S1, S2 and S3 are segments of the northern COB margin and S'1, S'2 and S'3 are conjugate segments on the southern SCS margin. From 10 to ~7 Ma, the portion of Ryukyu arc with the Yaeyama Islands (in brown) rotated simultaneously with the propagation of the tear fault T1 along S1. The three positions of Luzon Island (dotted lines) in Fig. 10D are extracted from Figs. 10A to 10C and show the change in HB-PSP/EU motion from a NNE direction between ~18 Ma and 10 Ma to a NE direction since 10 Ma. AP, Manila accretionary prism; DF, Deformation front; ELT, East Luzon Trough; EU, Eurasia; GR, Gagua ridge; HB, Huatung basin; I, Ishigaki Island; Ir, Iriomote Island; LOFZ, Luzon-Okinawa fracture zone; M, Miyako Island; MTF, Manila transcurrent fault; OT, Okinawa trough; PFZ, Philippine fault zone; PSP, Philippine Sea plate, TTZ, Taiwan transfer zone; Y, Yonaguni Island; YR, Yaeyama ridge.